OLD DOMINION UNIVERSITY RESEARCH FOUNDATION

DEPARTMENT OF MECHANICAL ENGINEERING AND MECHANICS
SCHOOL OF ENGINEERING
OLD DOMINION UNIVERSITY
NORFOLK, VIRGINIA

AERODYNAMIC PERFORMANCE OF SLENDER WINGS WITH SEPARATED FLOWS

By

C. Subba Reddy, Principal Investigator

Technical Report
For the period ending August 31, 1981

Prepared for the
National Aeronautics and Space Administration
Langley Research Center
Hampton, Virginia

Under
Research Grant NSG-1561
John E. Lamar, Technical Monitor
Transonic Aerodynamics Division

March 1982

Old Dominion University Research Foundation
P.O. Box 6369 • Norfolk, Virginia 23508-0369
Phone 804/440-4293

N82-22206

[redacted] grant change

May 4, 1982

Dr. John E. Lamar
Transonic Aerodynamics Division
National Aeronautics and Space Administration
Langley Research Center - Mail Stop 294
Hampton, VA 23665

Dear Dr. Lamar:

Enclosed please find three copies of the revised report cover and cover page for Dr. Reddy's March 1982 technical report on grant number NSG 1561. Please note that the date of the reporting period has been amended.

Also, please find enclosed three copies of figure 47, page 59. This page was left out of the original release by error.

I regret any inconvenience this might have caused you or your office. If you have any questions, please feel free to contact me.

Thank you,

Madelyn McRae

Madelyn McRae
Editor/Reports Coordinator

Encl: revised report cover, 3 cys
revised report cover page, 3 cys
figure 47, page 59, 3 cys

cc: ✓NASA Sci & Tech Info Fac, ltr
revised report cover, 2 cys
revised report cover page, 2 cys
figure 47, page 59, 2 cys

Dr. Reddy, ltr
revised report, 6 cys

Dr. Goglia, ltr
revised report cover, 1 cy
revised report cover page, 1 cy
figure 47, page 59, 1 cy

Dean Weese, ltr

ODU Library, ltr
revised report, 1 cy

Mr. Crowder, ltr

jan

DEPARTMENT OF MECHANICAL ENGINEERING AND MECHANICS
SCHOOL OF ENGINEERING
OLD DOMINION UNIVERSITY
NORFOLK, VIRGINIA

AERODYNAMIC PERFORMANCE OF SLENDER WINGS WITH SEPARATED FLOWS

By

C. Subba Reddy, Principal Investigator

Technical Report
For the period ending August 31, 1981

Prepared for the
National Aeronautics and Space Administration
Langley Research Center
Hampton, Virginia 23665

Under
Research Grant NSG-1561
John E. Lamar, Technical Monitor
Transonic Aerodynamics Division

Submitted by the
Old Dominion University Research Foundation
P.O. Box 6369
Norfolk, Virginia 23508-0369

March 1982

TABLE OF CONTENTS

LIST OF TABLES

LIST OF FIGURES

LIST OF FIGURES (CONTINUED)

LIST OF FIGURES (CONTINUED)

LIST OF FIGURES (CONCLUDED)

AERODYNAMIC PERFORMANCE OF SLENDER WINGS WITH SEPARATED FLOWS

By

C. Subba Reddy*

ABSTRACT

The aerodynamic performance of low-aspect ratio sweptback wings with vortex flows has been numerically investigated using the free vortex sheet method developed by Boeing Company. The models studied included flat, cambered, strake and leading-edge flapped wings of different planforms.

The theoretical results predicted by the method have been compared with the existing experimental data wherever available; and the code capabilities and limitations have been explored. Also the effects of the wing thickness, fuselage, leading-edge flap and multiple vortex modeling on the aerodynamic characteristics have been studied.

INTRODUCTION

This report briefly describes the research conducted under grant NSG 1561 during the period September 1, 1980 to August 31, 1981. In this work, mostly the latest version of the free vortex sheet (FVS) method of Boeing Company (refs. 1 and 2) has been employed to study various configurations not covered by the previous reports (refs. 3, 4 and 5), with a view to determining the code capabilities and limitations. Also the recently incorporated code capability for modeling wings with multiple vortex systems has been utilized on double delta wings. The quasi-vortex lattice (QVL) method of Mehrotra (refs. 6 and 7) and the vortex lattice method with the suction analogy (VLM-SA) of NASA-Langley Research Center (refs. 8, 9 and 10) which were extensively used in previous studies (refs. 3 and 4) have rarely been employed in this investigation. The models studied included flat, cambered,

*Assistant Professor, Department of Mechanical Engineering and Mechanics, Old Dominion University, Norfolk, Virginia 23508.

strake, and leading-edge flapped wings of different planforms. The details of these planforms are given in table 1. In the following sections, the results are discussed and some of the code capabilities and limitations are evaluated.

NOMENCLATURE

A	aspect ratio
b	wing span
b(x)	local wing span
c	local wing chord
$\bar{c}$	mean aerodynamic chord
c_r	wing root chord
C_D	drag coefficient
ΔC_D	drag due-to-lift coefficient
C_L	lift coefficient
C_m	pitching moment coefficient
ΔC_p	net lifting pressure coefficient
FVS	free vortex sheet
M	Mach number
QVL	quasi-vortex lattice
VLM-SA	vortex lattice method coupled with the suction analogy
x,y,z	body axis coordinates
α	angle of attack
δ_n	leading-edge flap angle normal to hinge, positive angle represents flap deflected downwards

RESULTS AND DISCUSSION

In this section, the results obtained by using the FVS method are compared wherever possible with existing data, and also with the results given by the quasi-vortex lattice method (refs. 6 and 7) and some of the code capabilities and limitations are discussed. Also the effects of fuselage, wing thickness and leading-edge flaps on the aerodynamic performance of wings are theoretically studied by carrying out extensions beyond existing data using the FVS method.

A summary of the various wing configurations investigated using the code is presented in table 1. The range of angles of attack over which the code is employed and whether or not the solutions are converged are also indicated in the table. In this report, the wings are considered to have no thickness or yaw unless otherwise stated.

Figures 1 to 3 show the comparison between the results predicted by the FVS and QVL methods and the experimental data (ref. 11) for an apex cambered delta wing. Though the longitudinal aerodynamic characteristics given by both the methods are in fairly good agreement with the data as shown in figure 1, there is no such agreement in the case of spanwise pressure distributions as evidenced by figures 2 and 3. However, the FVS method provides better pressure distributions than the QVL method.

An 80°/65° flat double delta wing (ref. 12) is modeled, as shown in figures 4 to 6, in three ways: (1) with a single vortex system all along the leading-edge, (2) with separated flow on inboard leading-edge and attached flow on outboard leading edge, and (3) with two separate vortex systems on inboard and outboard leading edges. The theoretical results obtained in the above three cases are compared with the experimental data (ref. 12) for the delta wing in figure 7. The double vortex modeling provides better agreement with the data as expected, especially in case of pitching moment whereas the model with single vortex only on the inboard leading edge gives the results that agree poorly. From this, it is clear that the separated flow on the outboard leading edge has considerable effect on the overall aerodynamic performance characteristics of a double delta wing. Figures 8 and 9 show converged vortex sheet shapes for the three cases at different chordwise stations and angles of attack. They show that vortex sheet sizes

become bigger as $\frac{x}{c_r}$ and α increase as expected. The spanwise pressure distributions at different chordwise stations and angles of attack for the three cases are illustrated in figures 10-13. The pressures on the bottom surface are essentially the same in all the three cases whereas upper surface pressures differ significantly in terms of magnitude and peak locations. The two-vortex system modeling gives two pressure peaks in the aft region of the wing as expected. In the case of modeling with separated flow on the inboard leading edge and attached flow on the outboard leading edge, the pressure is very high at the outboard leading edge. This is in accordance with the theory.

In figure 14, the results obtained by the FVS method are compared with the data (ref. 13) for a flat double arrow wing configuration. The near-wake modeling provides the results that agree better with the data than those predicted by non-near-wake modeling. It may be noted here that the near-wake in this case is confined to the notch portion only, and the tip edge of the SCAT-15F model is approximated to a point for facilitating solution convergence. Figure 15 shows the converged vortex sheet shapes at two angles of attack and chordwise stations for the above wing.

No converged results could be obtained for SCAT-15F (ref. 14) wing when double vortex system or a single vortex on inboard leading edge only are used. When the wing is approximated to a double delta by eliminating the sweep on trailing edge, the FVS method gives converged results for the latter case. The spanwise pressure distributions for such a wing are shown in figure 16.

In order to determine the effect of fuselage on the aerodynamic performance of SCAT-15F model, wing-body combination configuration is considered as shown in figure 17. Source type networks are used to represent the body and doublet-type networks for the wing. The spanwise pressure distributions obtained by modeling with and without body are compared in figures 18 and 19. The effect of the body is to move the pressure peak location outboard as shown in the figures. However, the body effect on the longitudinal aerodynamic characteristics is not appreciable as indicated in table 2.

When the camber is considered and the leading edge is not lined up in modeling the SCAT-15F wing using the FVS method, no solution convergence is obtained. However, a convergence is achieved when the leading edge is sheared (leading edge is lined up keeping the slopes at control points on the camber surface the same). But the agreement between the results so predicted and the data (ref. 15) is poor as indicated by figure 20. The spanwise pressure distributions for the above wing (cambered and leading edge sheared) are shown in figures 21 and 22.

In order to determine the effect of wing thickness on the aerodynamic performance of SCAT-15F wing, it is modeled as shown in figure 23. Though this thick wing modeling gives a converged solution, the predicted results are very much different from the data and also from the results obtained in thin wing modeling. However, it may be appropriate to mention here that it has subsequently been pointed out that there was some error in programming the source panels used to model thickness.

The NASA/Boeing vortex flap configuration which is essentially a cropped double arrow wing with leading-edge vortex flaps could not be successfully modeled by the FVS method even after making several approximations to the planform.

A 74° flat delta wing with a 2 in. conical leading edge vortex flap is modeled for various upward and downward flap deflections. The converged results are shown in figures 24 to 46. The reference area used here is the area of the basic wing plus the actual area of the flaps in all the cases except in figure 24 where it is the basic wing area only.

Figure 24 shows the comparison of predicted aerodynamic characteristics with the data (ref. 16) for an upward flap deflection of 130°. As the figure shows the agreement between them is fairly good.

The converged vortex sheet shapes at two chordwise stations are shown in figures 25 to 30 for several flap deflections, and spanwise pressure distributions in figures 31 to 44. In some cases the pressures on wing and flap are separately shown for clarity. In plotting these pressures, the spanwise distance is nondimensionalized by the local span of the basic wing

only. The effect of the flap deflection angle on the longitudinal aerodynamic characteristics are shown in figures 45 and 46, and the flow pattern over the wing in figure 47 is illustrated.

CONCLUSIONS

The aerodynamic characteristics of highly sweptback wings with vortex flows have been investigated using the numerical code developed by Boeing Company. Wings of different planforms have been studied and the predicted results compared with the existing experimental data wherever possible, in order to determine the code capabilities and limitations. Also in some cases, the code has been employed to study the effects of wing thickness, fuselage, leading-edge flap and multiple vortex system modeling on the aerodynamic performance of the wings.

The code generally provides the overall aerodynamic characteristics that agree fairly well with the experimental data for most of the planforms studied. However, the predicted spanwise pressure distributions are not in good agreement with the data. Also the code could not provide a converged solution for a cambered wing whose leading edge is not lined up. When the leading edge was lined up, the method could give a converged solution but the results are poor.

The multiple vortex modeling on double delta wing provides better results than a single vortex modeling but the rate of convergence is slower. When this multiple vortex modeling is used for a double arrow wing, no converged solution can be obtained. It appears from this that the sweptback trailing edge is hindering the convergence process. The method also fails to give converged solution with two vortices--one starting from the end of leading-edge flap and another from the hinge line--in case of a 74° delta wing with leading-edge flap.

REFERENCES

1. Johnson, F.T.; Lu, P.; Tinoco, E.N.; and Epston, M.A.: An Improved Panel Method for the Solution of Three-Dimensional Leading-Edge Vortex Flows. Volume I - Theory Document. NASA CR-3278, 1980.

2. Tinoco, E.T.; Lu, P.; and Johnson, F.T.: An Improved Panel Method for the Solution of Three-Dimensional Leading-Edge Vortex Flows. Volume II - User's Guide and Programmer's Document. NASA CR-3279, 1980.

3. Reddy, C.S.: Theoretical Study of Aerodynamic Characteristics of Wings Having Vortex Flow. NASA CR-159184, 1979.

4. Reddy, C.S.: Investigation of Aerodynamic Characteristics of Wings Having Vortex Flow Using Different Numerical Codes. NASA CR-165706, 1981.

5. Reddy, C.S.: Numerical Study of Aerodynamic Characteristics of Swept-back Wings Having Vortex Flows. Progress Report for NASA Grant NSG 1561, 1980.

6. Mehrotra, S.C.: A Theoretical Investigation of the Aerodynamics of Low Aspect-Ratio Wings with Partial Leading-Edge Separation. NASA CR-145304, 1978.

7. Mehrotra, S.C.; and Lan, C.E.: A Computer Program for Calculating Aerodynamic Characteristics of Low-Aspect Ratio Wings with Partial Leading-Edge Separation. NASA CR-145362, 1978.

8. Polhamus, E.C.: A Concept of the Vortex Lift of Sharp-Edge Delta Wings Based on a Leading-Edge Suction Analogy. NASA TN D-3767, 1966.

9. Margason, R.J.; and Lamar, J.E.: Vortex-Lattice Fortran Program for Estimating Subsonic Aerodynamic Characteristics of Complex Planforms. NASA TN-D-6142, 1971.

10. Lamar, J.E.; and Gloss, B.B.: Subsonic Aerodynamic Characteristics of Interacting Lifting Surfaces with Separated Flow Around Sharp Edges Predicted by a Vortex-Lattice Method. NASA TN D-7921, 1975.

11. Wentz, W.H.: Effects of Leading-Edge Camber on Low Speed Characteristics of Slender Delta Wings. NASA CR-2002, 1972.

12. Lamar, J.e.: Analysis and Design of Strake-Wing Configurations. J. Aircraft, Vol. 17, No. 1, 1980, pp. 20-27.

13. Freeman, D.C., Jr.: Low Subsonic Flight and Force Investigation of a Subsonic Transport Model with a Highly Swept Arrow Wing. NASA TN D-3887, 1967.

14. Morris,O.A.; and Fournier, R.H.: Aerodynamic Characteristics at Mach Numbers 2.30, 2.60 and 2.96 of a Supersonic Transport Model Having a Fixed, Warped Wing. NASA TM X-1115.

15. Henderson, W.P.: Unpublished data obtained at NASA-Langley Research Center.

16. Rao, D.M.: Unpublished data obtained at NASA-Langley Research Center.

Table 1. Wing configurations modeled by the FVS method.

Serial Number	Wing Description	Angle of Attack	Solution Converged?
1	74° apex cambered delta wing, A = 1.15 (ref. 11)	10°	no
2	74° apex cambered delta wing, A = 1.15 (ref. 11)	15°-30°	yes
3	80°/65° flat double delta wing, A = 1.60 (ref. 12) (vortex on inboard leading edge only)	10°-25°	yes
4	80°/65° flat double delta wing, A = 1.60 (ref. 12) (single vortex on entire leading edge)	15°-30°	yes
5	80°/65° flat double delta wing A = 1.60 (ref. 12) (two separate vortices on inboard and outboard leading edges	10°-25°	yes
6	74°/65° flat double arrow wing (SCAT-15F), A = 1.72 (ref. 13) (single vortex on entire leading edge; with and without near wake)	8°-25°	yes
7	74°/65° flat double arrow wing (SCAT-15F), A = 1.72 (ref. 14) (vortex on inboard leading edge only; with and without near wake	20°	no
8	The above wing (No. 7) with unswept trailing edge	20°	yes
9	74°/65° flat double arrow wing (SCAT-15F), A = 1.72 (ref. 14) (Two separate vortices on inboard and outboard leading edges; with and without near wakes)	20°	no
10	The above wing (No. 9) with unswept trailing edge	20°	yes

(cont'd)

Table 1. (Continued).

Serial Number	Wing Description	Angle of Attack	Solution Converged?
11	74°/65° flat double arrow wing (SCAT-15F), A = 1.72 (ref. 14) (single vortex on entire leading edge; wing-body combination; near wake)	15°,20°	yes
12	74°/65° cambered double arrow wing (SCAT-15F), A = 1.72 (ref. 14) (single vortex on entire leading edge that is not lined up; with near wake)	20°	no
13	The above wing (No. 12) with lined-up leading edge	10°-25°	yes
14	The above wing (No. 13) with its thickness considered	20°	yes
15	75°/60° NASA-Boeing leading-edge vortex flap model, A = 1.47	12.9°,20°	no
16	74° flat delta wing with 2" conical leading-edge vortex flap deflected through δ_n = 0° to ±110°	20°	yes
17	74° flat delta wing with 2" conical leading-edge vortex flap deflected through δ_n = 120°-170°	20°	no
18	74° flat delta wing wing 2" conical leading-edge vortex flap deflected through δ_n = -140° to - 170°	20°	no
19	74° flat delta wing with 2" conical leading-edge vortex flap deflected through δ_n = -130°	<5°	no

(cont'd)

Table 1. (Concluded).

Serial Number	Wing Description	Angle of Attack	Solution Converged?
20	74° flat delta wing with 2" conical leading-edge vortex flap deflected through δ_n = -130°	5°-25°	yes
21	74° flat delta wing with 2" conical leading-edge vortex flap deflected through δ_n = -120°	20°	yes
22	The above wing (No. 21) with two vortices (one on the flap and another on the wing)	20°	no
23	74° flat delta wing with no flap	5°-25°	yes
24	74° flat delta wing with 2" rectanglar leading-edge vortex flap deflected through δ_n = 0° to -60°	20°	yes
25	74° flat delta wing with 2" rectangular leading-edge vortex flap deflected through δ_n = 0° to 20°	20°	yes
26	The above wing (No. 25) with δ_n > -40°	20°	no

Table 2. Effect of body on the aerodynamic characteristics of double arrow wing; M = 0.2

α	Aerodnyamics Characteristics	Modeling Type	
		Without Body	With Body
10°	C_L	0.3549	0.3476
"	ΔC_D	0.0626	0.0608
"	C_m	0.0153	0.0228
15°	C_L	0.5411	0.5333
"	ΔC_D	0.1450	0.1418
"	C_m	0.0583	0.0683
20°	C_L	0.7557	0.7574
"	ΔC_D	0.2751	0.2738
"	C_m	0.1032	0.1128

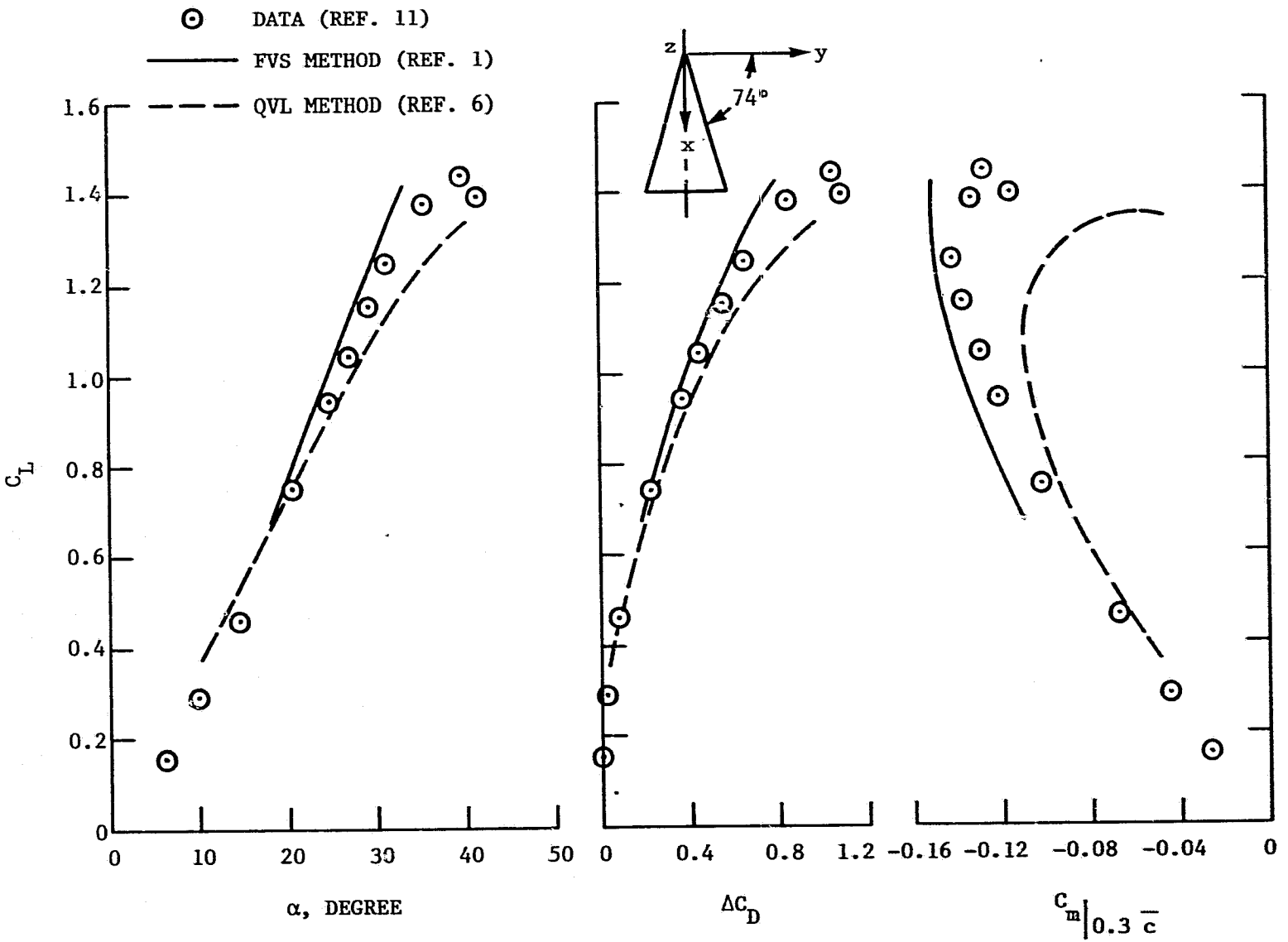

Figure 1. Longitudinal aerodynamic characteristics of A = 1.15 apex cambered delta wing at $M \approx 0$.

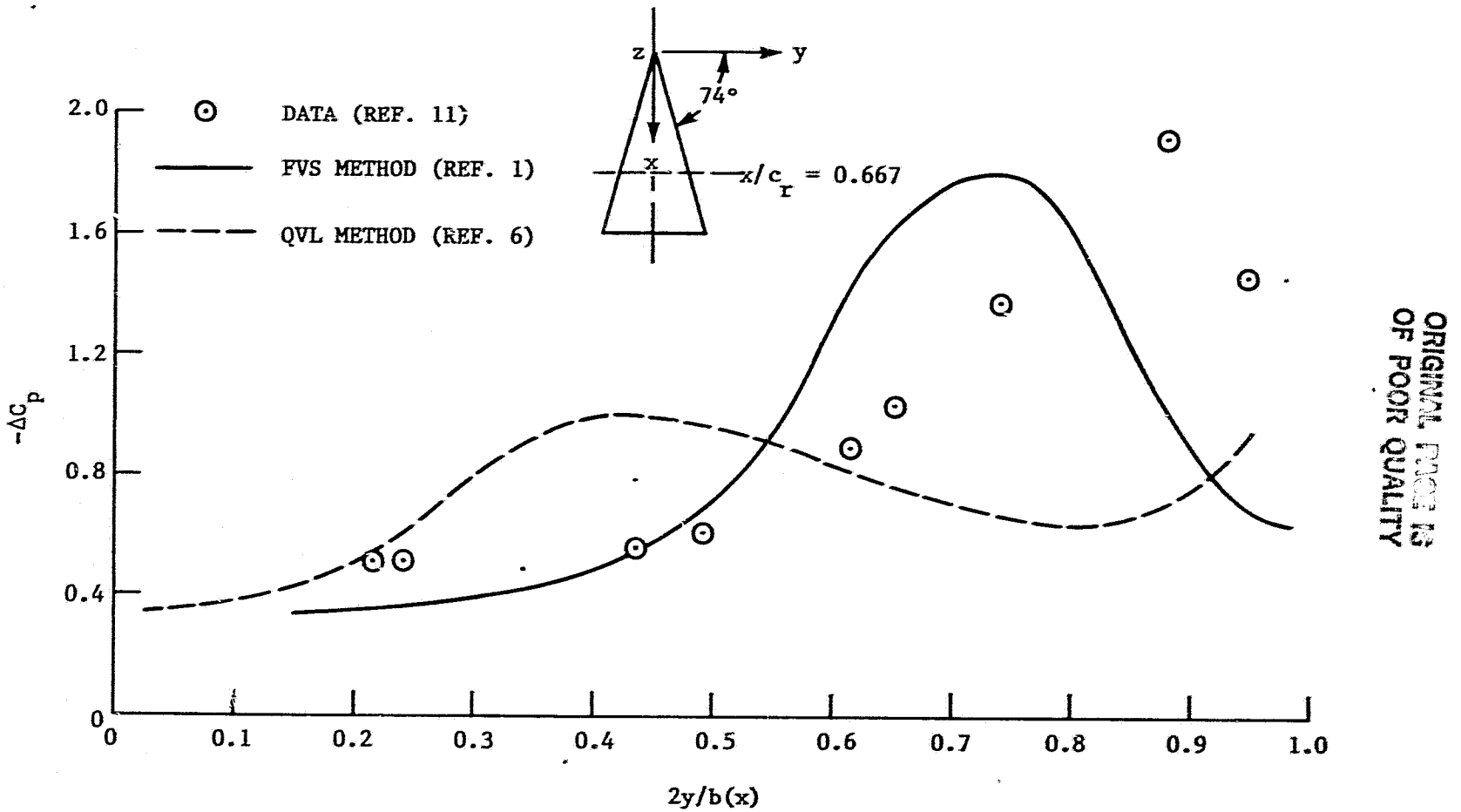

Figure 2. Spanwise pressure distribution for A = 1.15 apex cambered delta wing at $\alpha = 20°$ and $M \approx 0$.

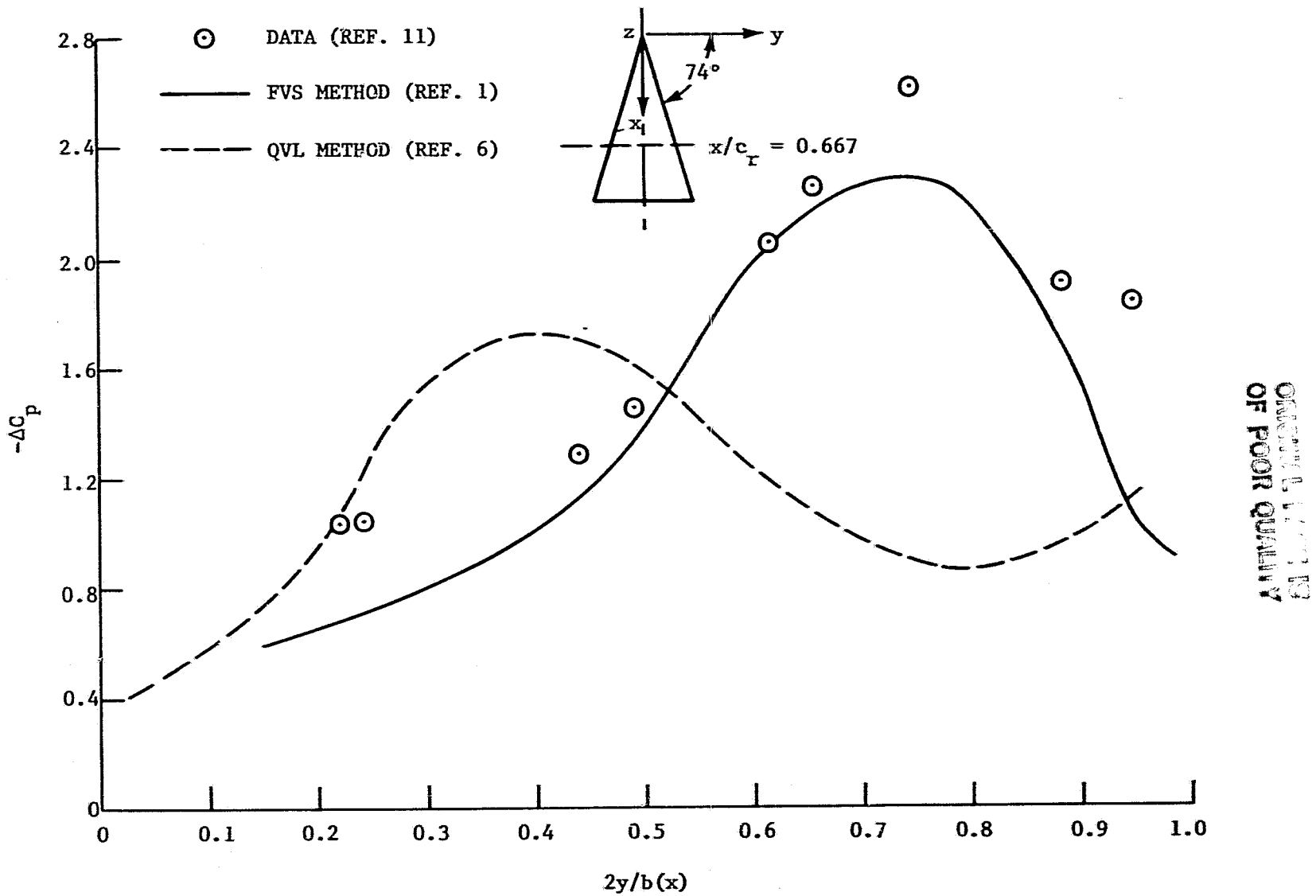

Figure 3. Spanwise pressure distribution for A = 1.15 apex cambered delta wing at $\alpha = 30°$ and $M \approx 0$.

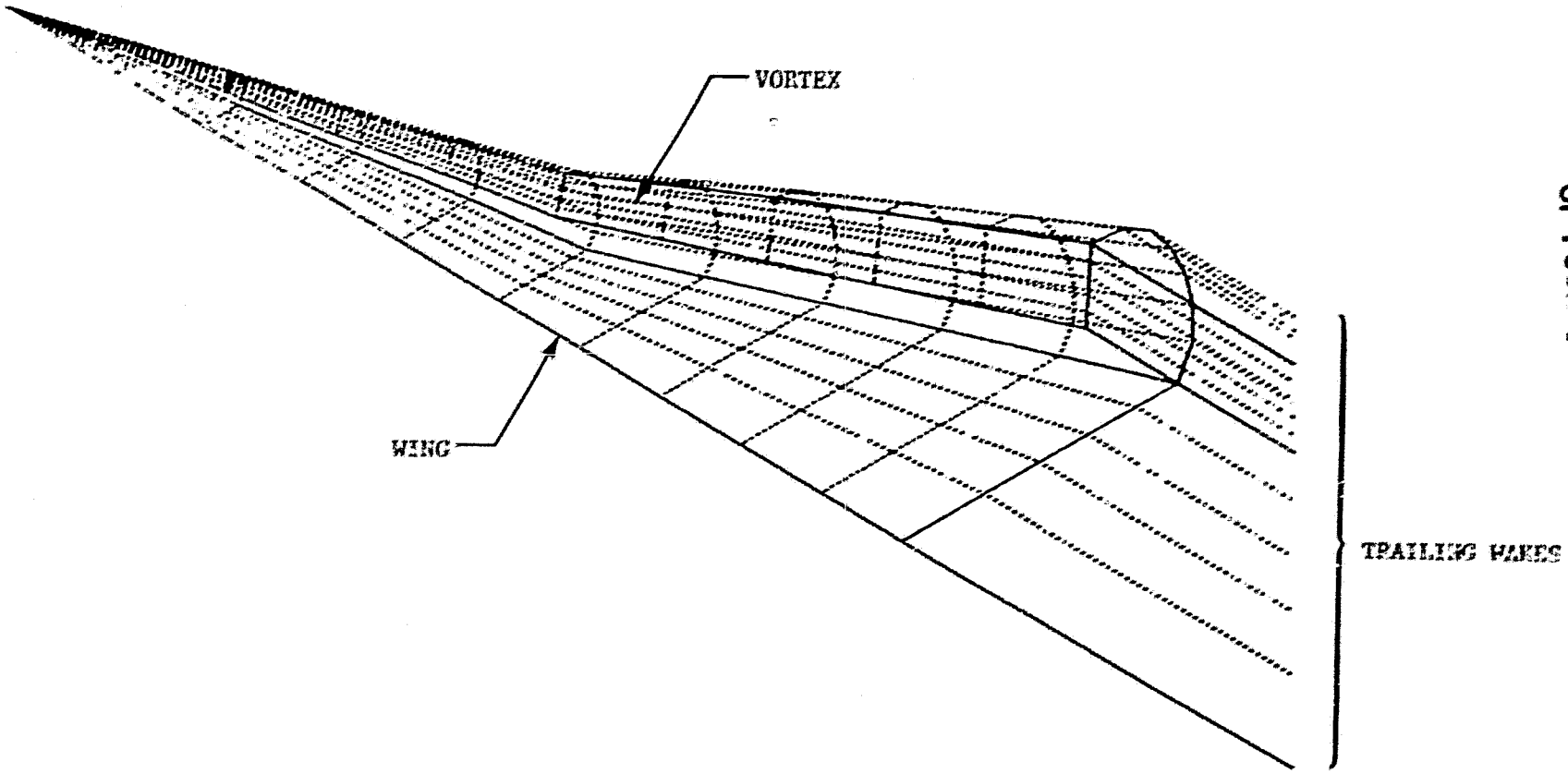

Figure 4. Flat double delta wing with single vortex on entire leading edge.

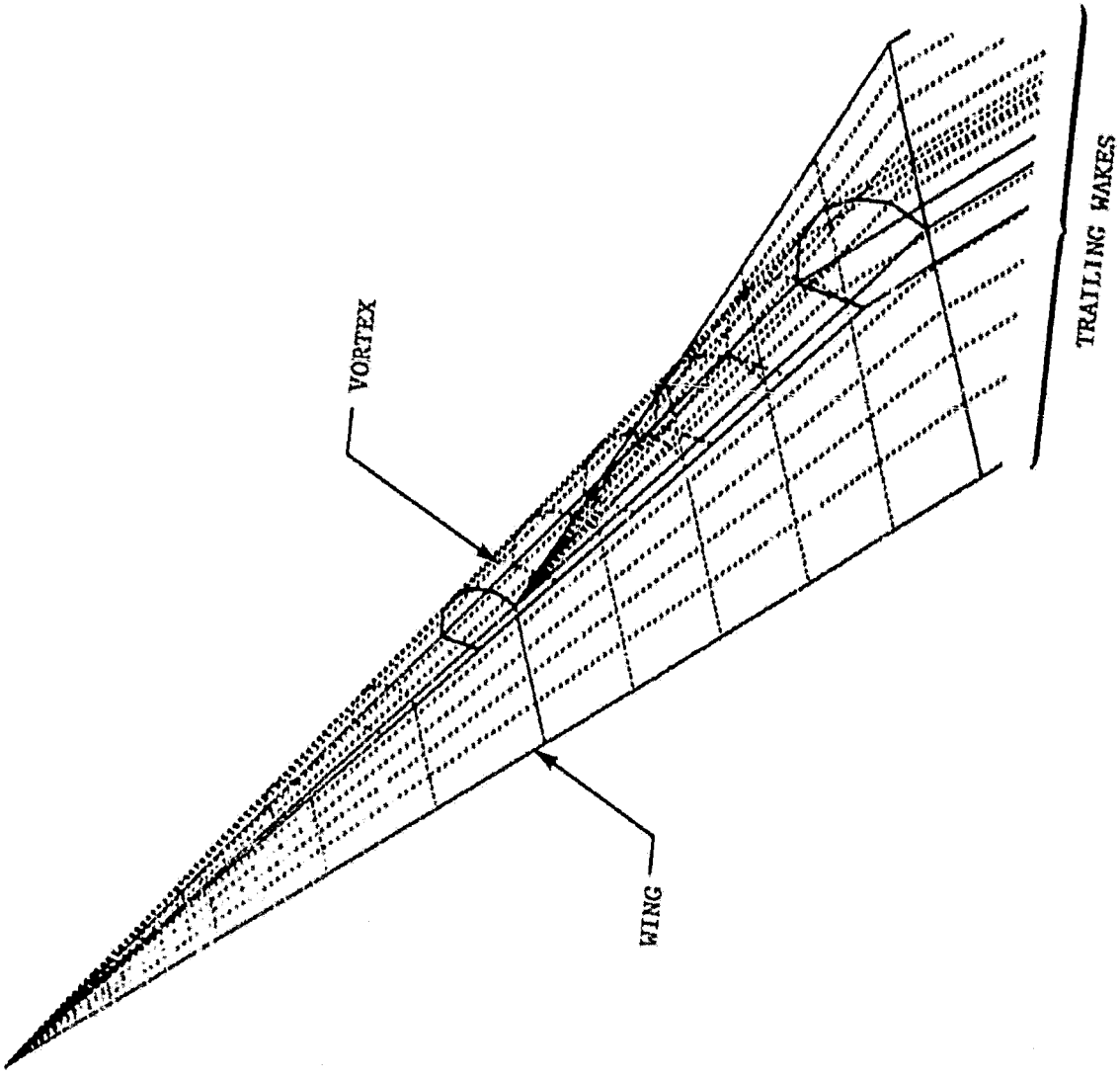

Figure 5. Flat double delta wing with vortex on inboard leading edge only.

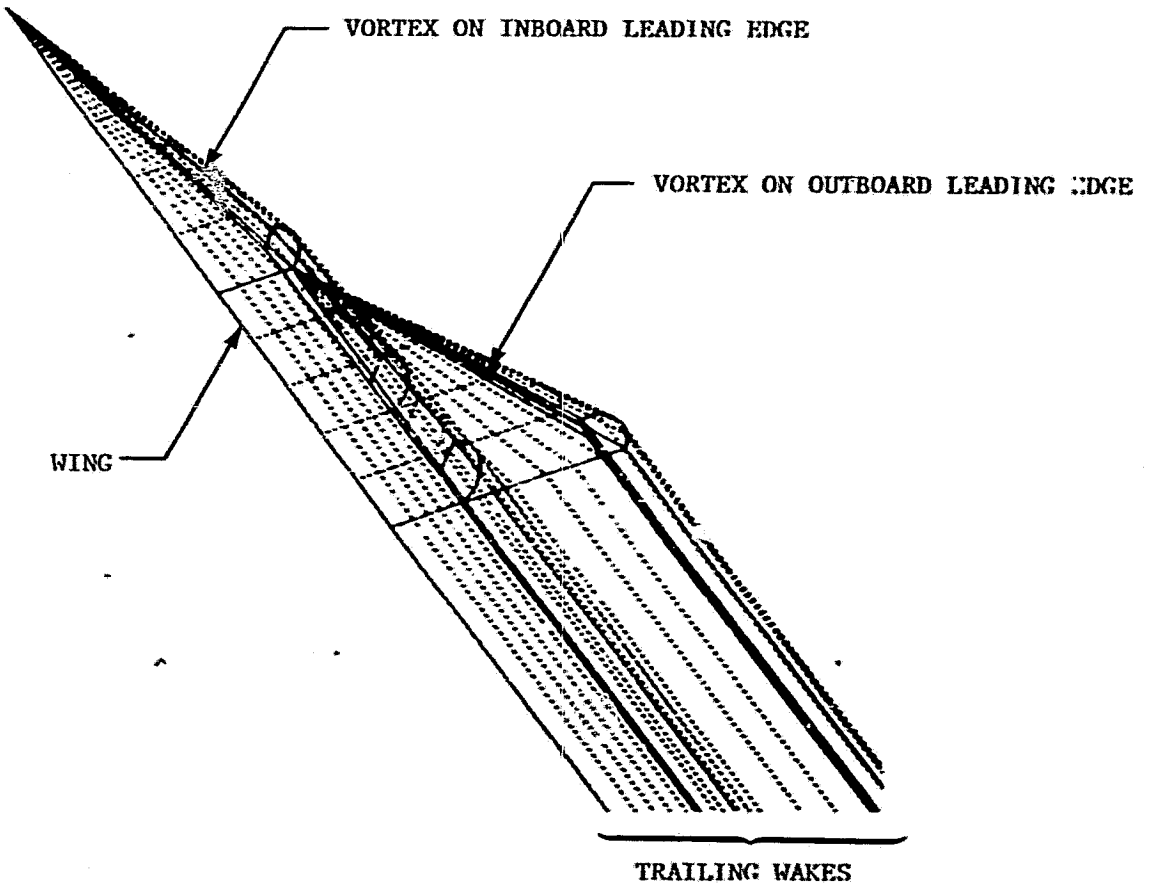

Figure 6. Flat double delta wing with two separate vortex systems on inboard and outboard leading edges.

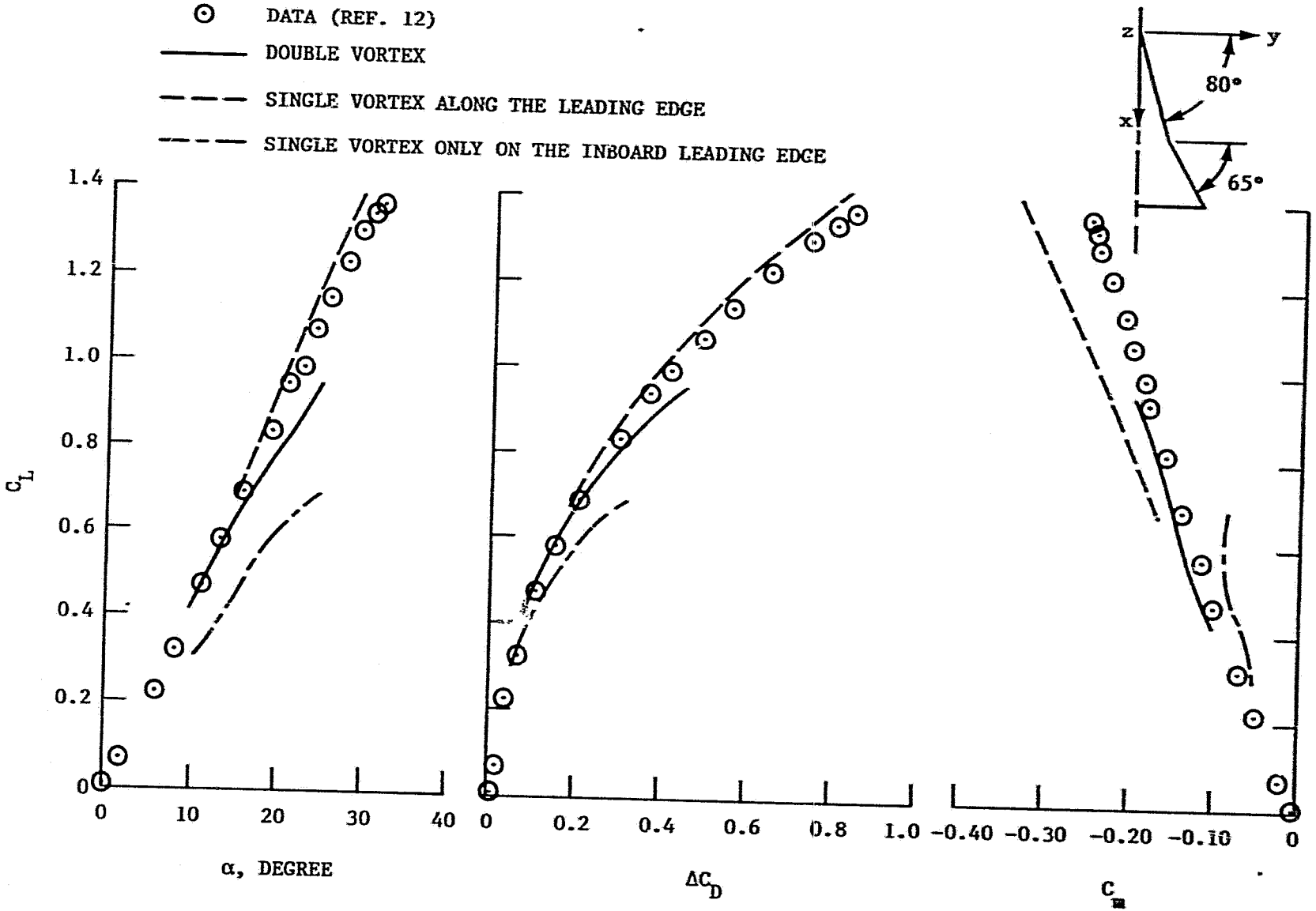

Figure 7. Longitudinal aerodynamic characteristics of A = 1.60 flat double delta wing at M ≈ 0.

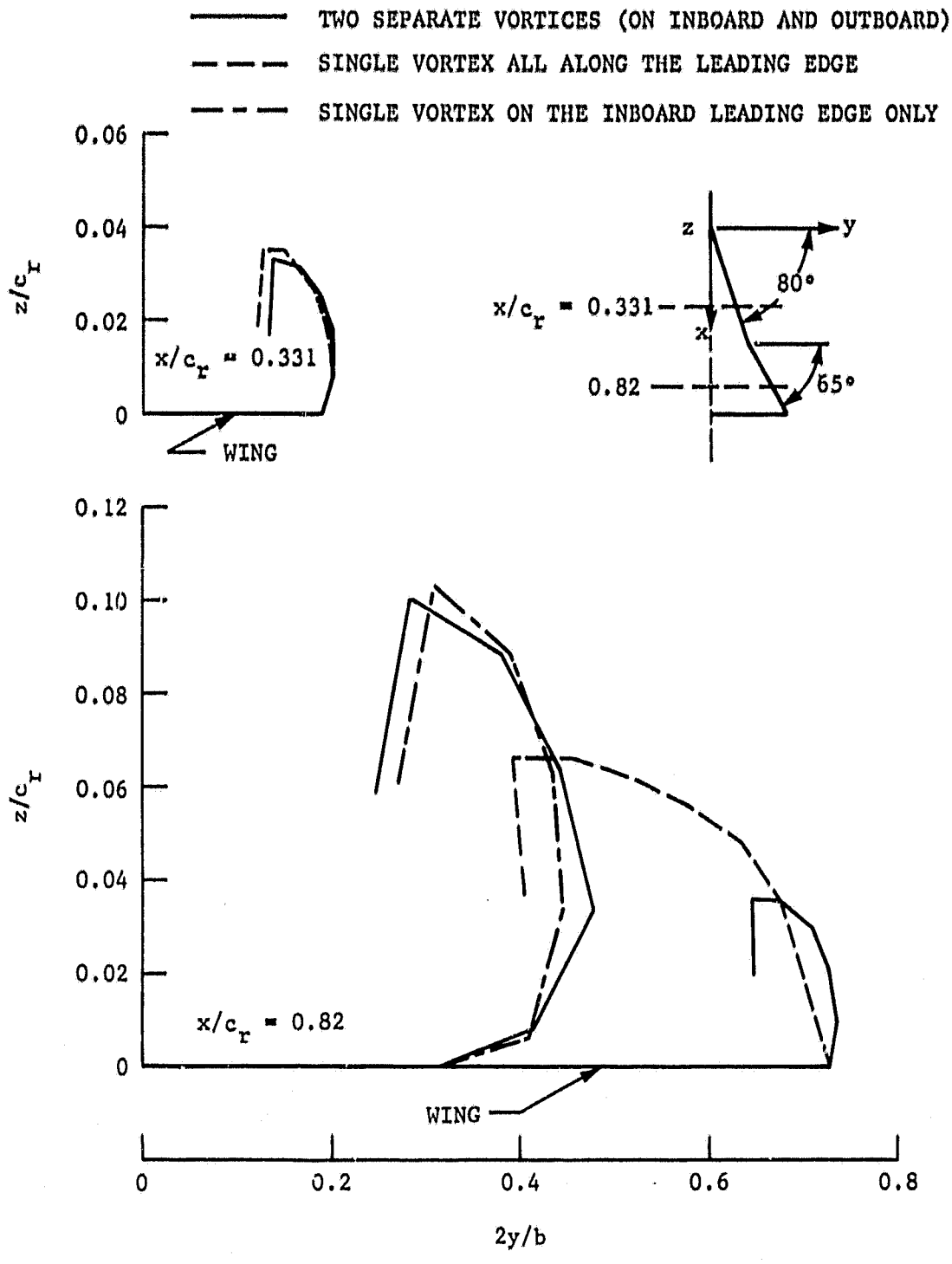

Figure 8. Converged shapes of different vortex systems for A = 1.60 flat double delta wing at $\alpha = 15°$, M = 0.

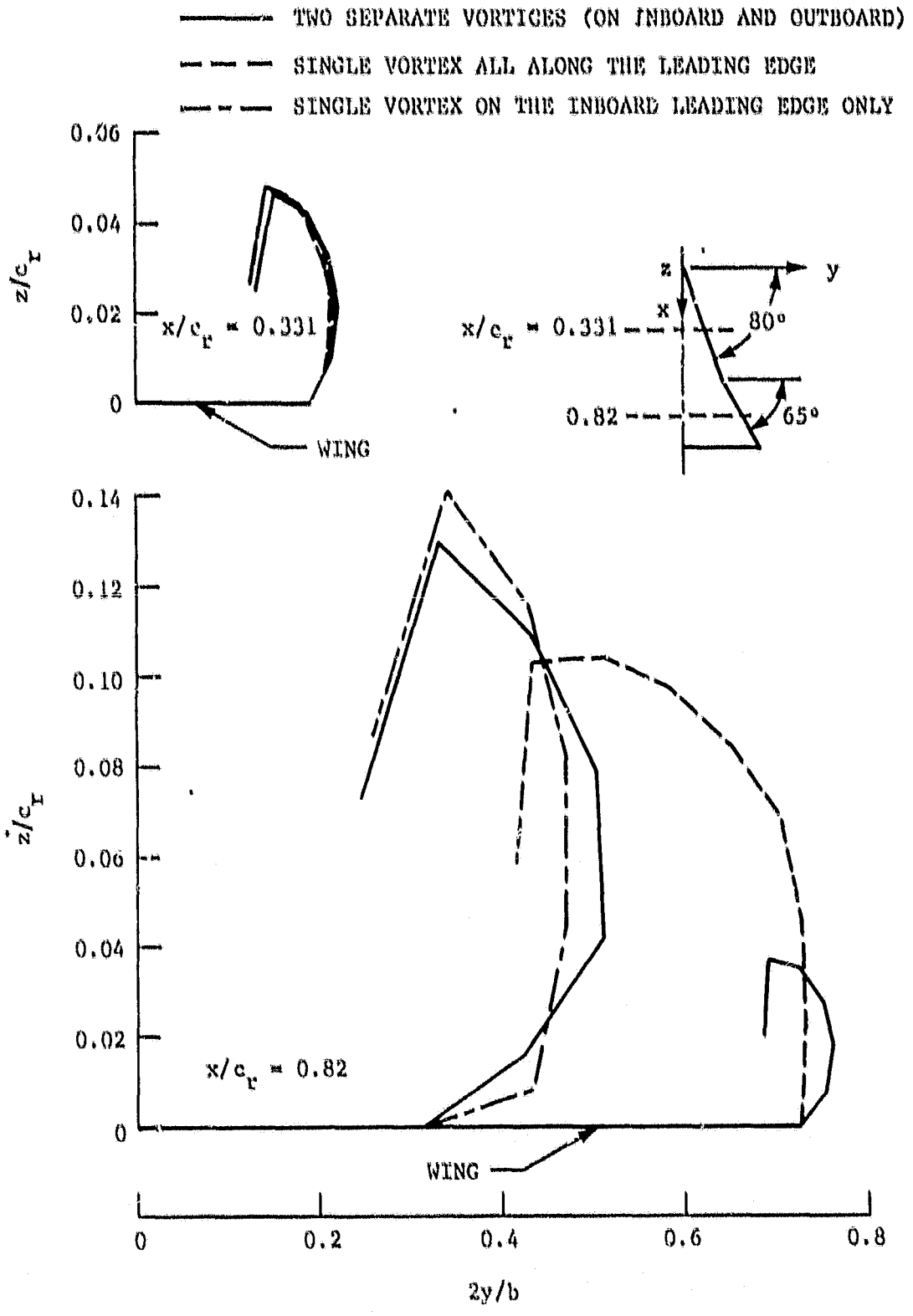

Figure 9. Converged shapes of different vortex systems for $\Lambda = 1.60$ flat double delta wing at $\alpha = 25°$, $M = 0$.

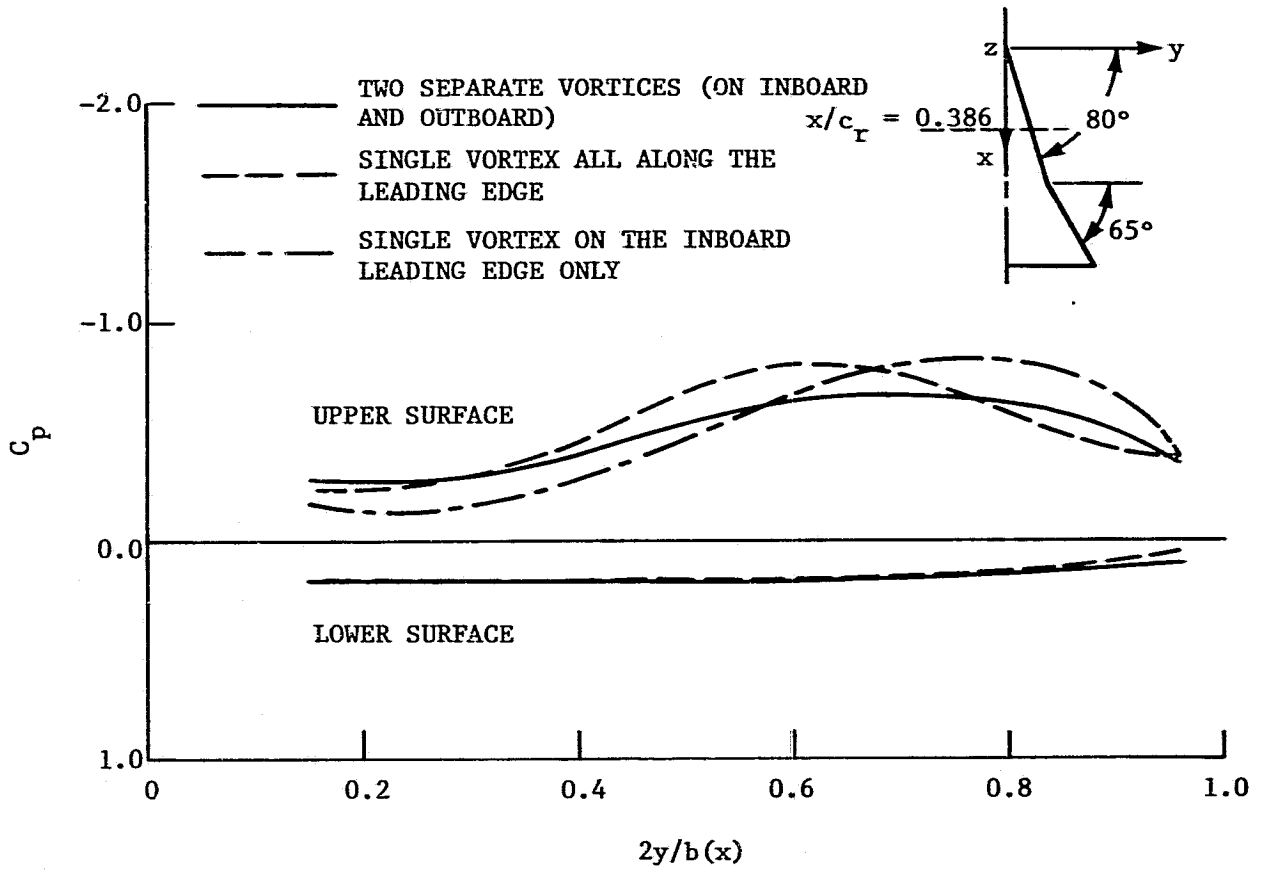

Figure 10. Effect of different vortex systems on spanwise pressure distributions for A = 1.60 flat double delta wing at x/c_r = 0.386, α = 15° and M = 0.

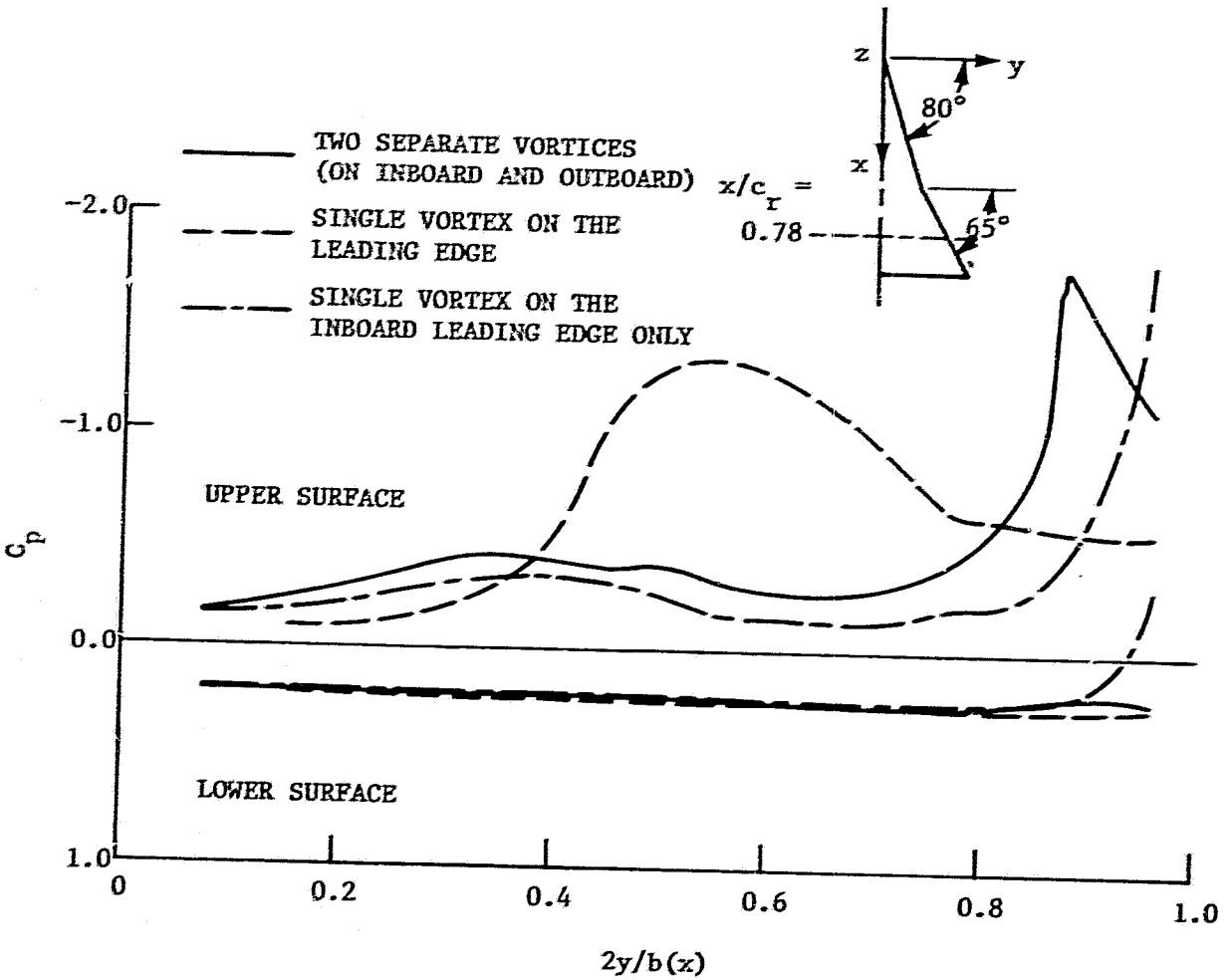

Figure 11. Effect of different vortex systems on spanwise pressure distributions for A = 1.60 flat double delta wing at $x/c_r = 0.78$, $\alpha = 15°$ and M = 0.

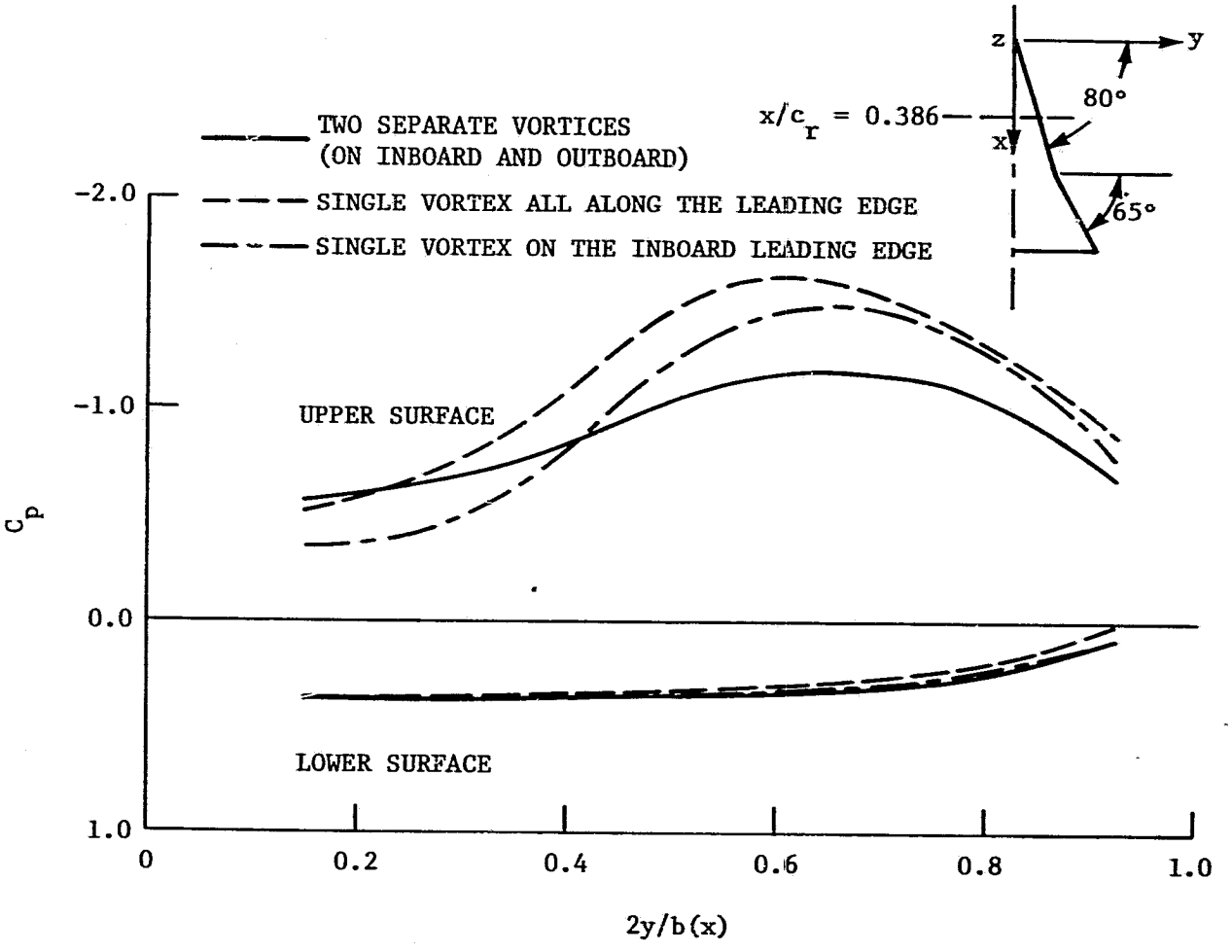

Figure 12. Effect of different vortex systems on spanwise pressure distributions for A = 1.60 flat double delta wing at $x/c_r = 0.386$, $\alpha = 25°$ and M = 0.

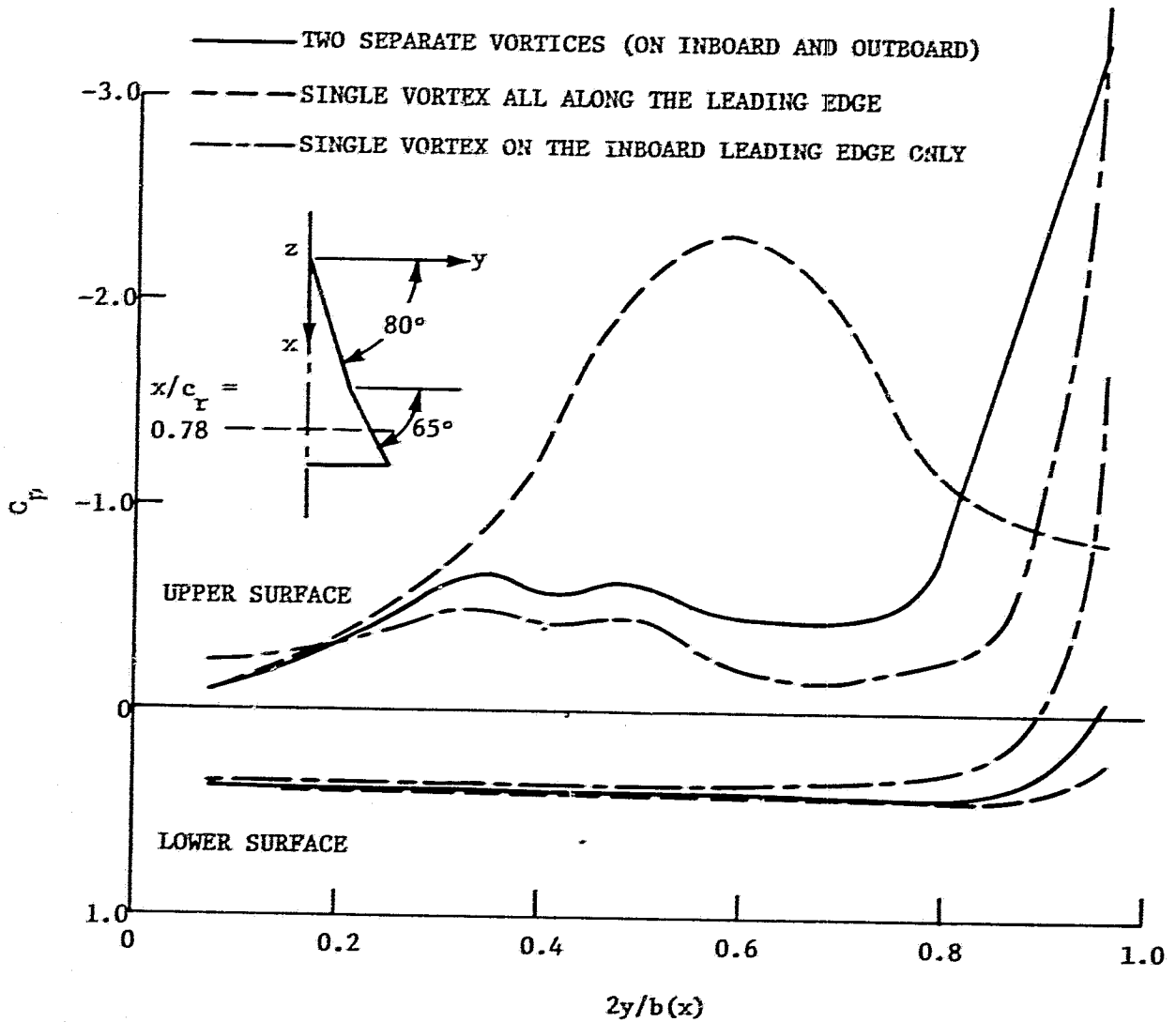

Figure 13. Effect of different vortex systems on spanwise pressure distributions for A = 1.60 flat double delta wing at x/c_r = 0.78, α = 25° and M = 0.

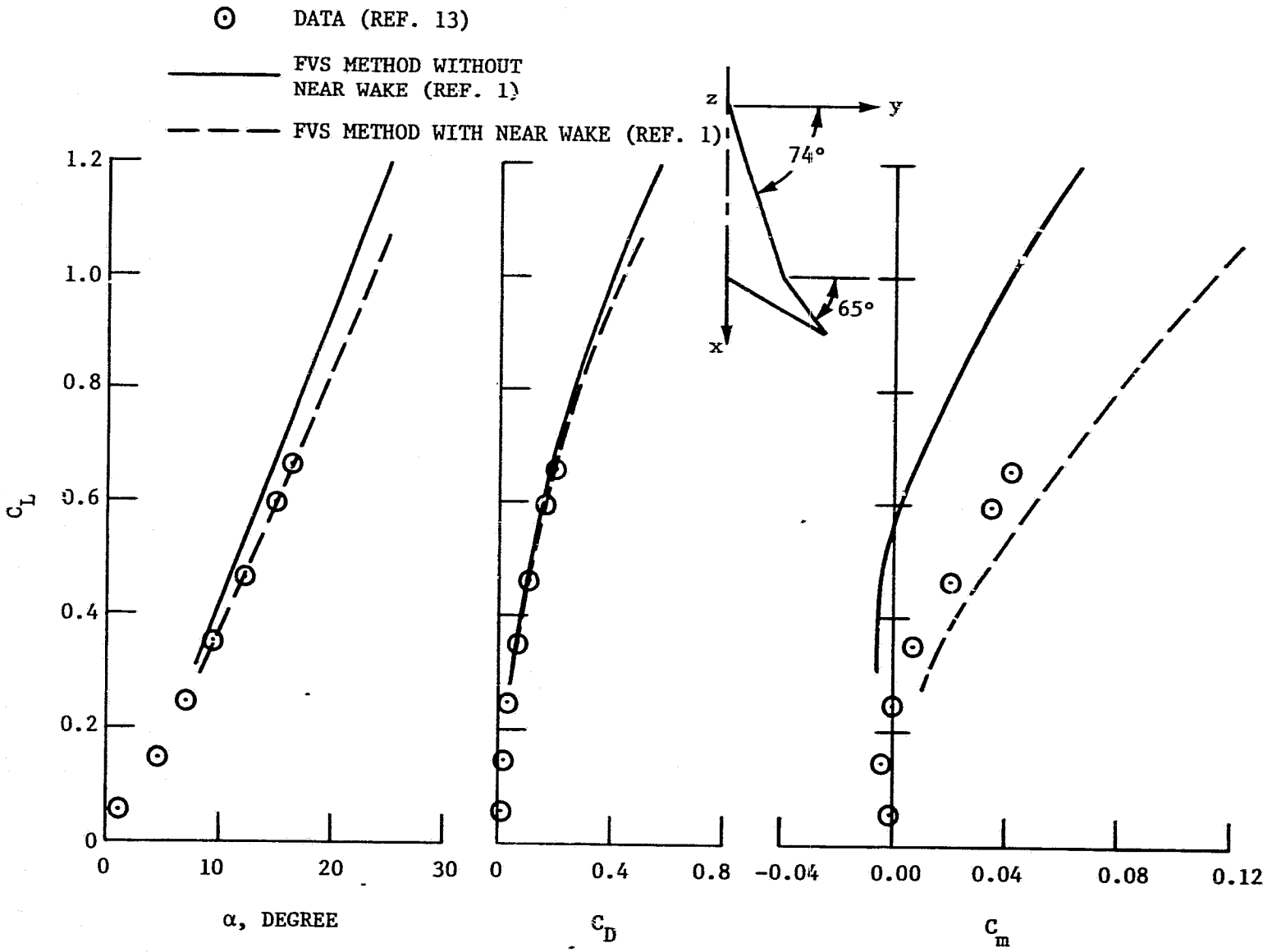

Figure 14. Aerodynamic characteristics of A = 1.72 flat double arrow wing (SCAT-15F) at M = 0.2.

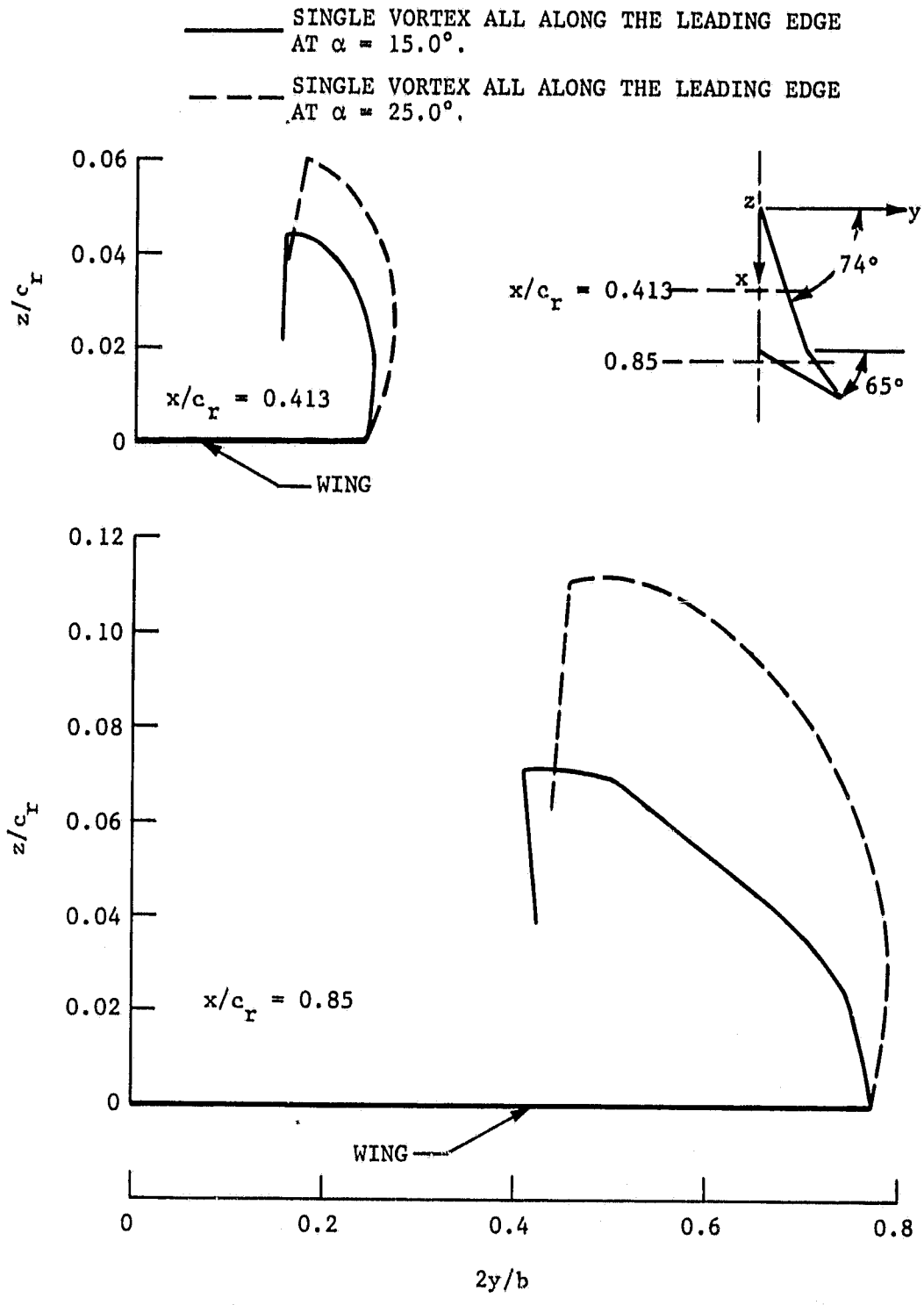

Figure 15. Converged shapes of vortex systems for A = 1.72 flat double arrow (SCAT-15F) at different angles of attack and M = 0.2.

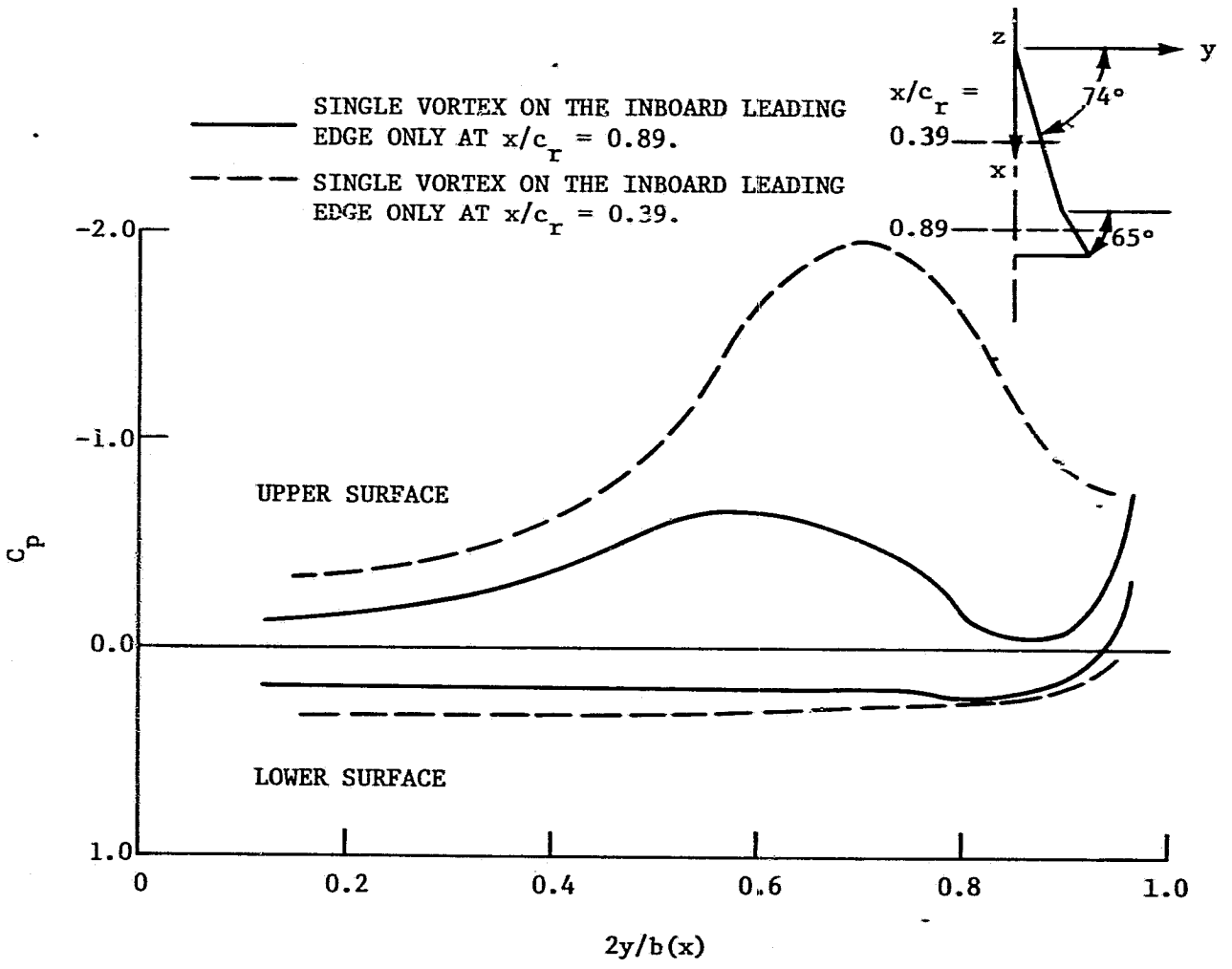

Figure 16. Spanwise pressure distributions for A = 1.45 flat double delta wing with vortex only on the inboard leading edge at $\alpha = 20°$ and M = 0.2.

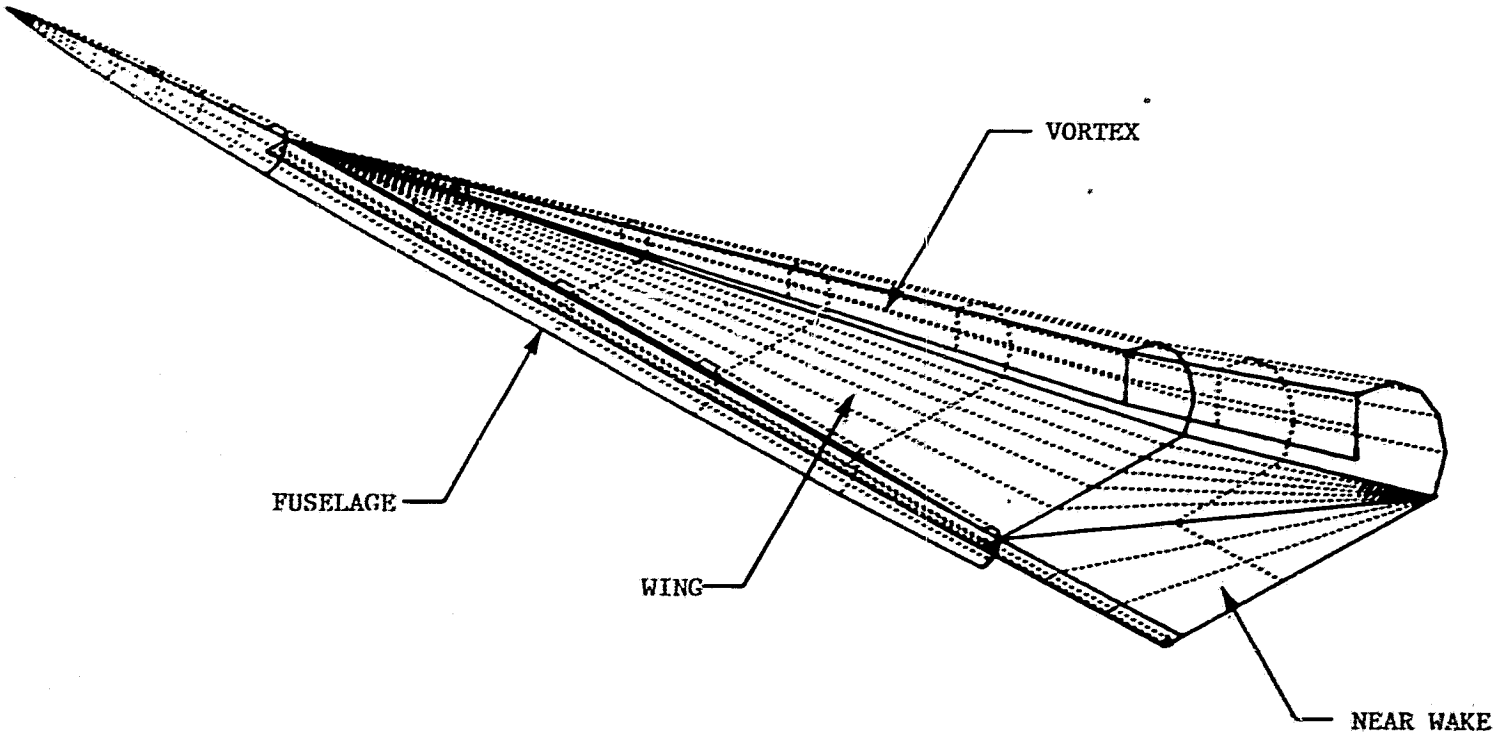

Figure 17. Wing-body combination of flat double arrow wing (SCAT-15F).

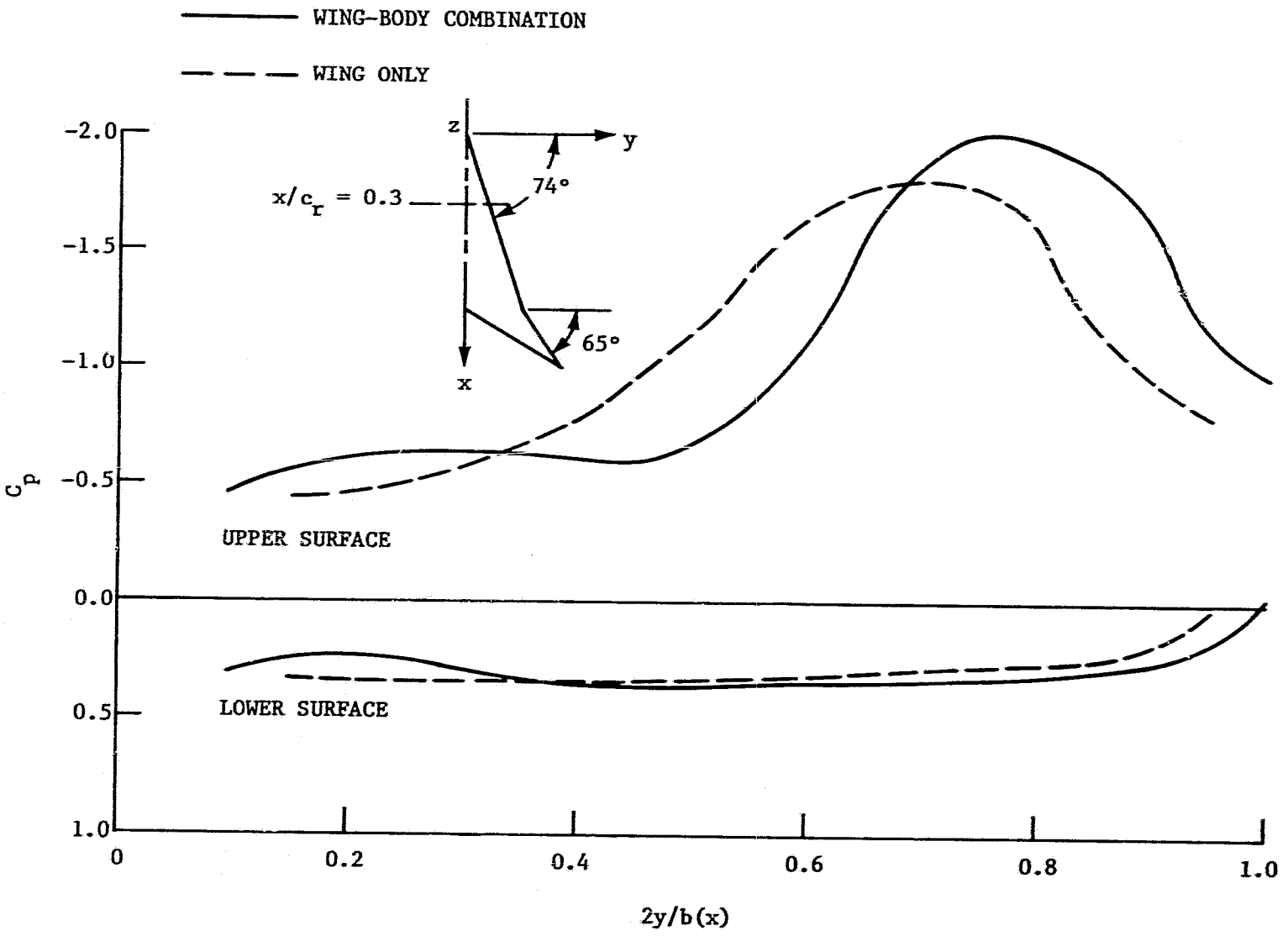

Figure 18. Comparison of spanwise pressure distributions for A = 1.72 flat double arrow wing (SCAT-15F) with and without body at $x/c_r = 0.30$, $\alpha = 20°$ and M = 0.2.

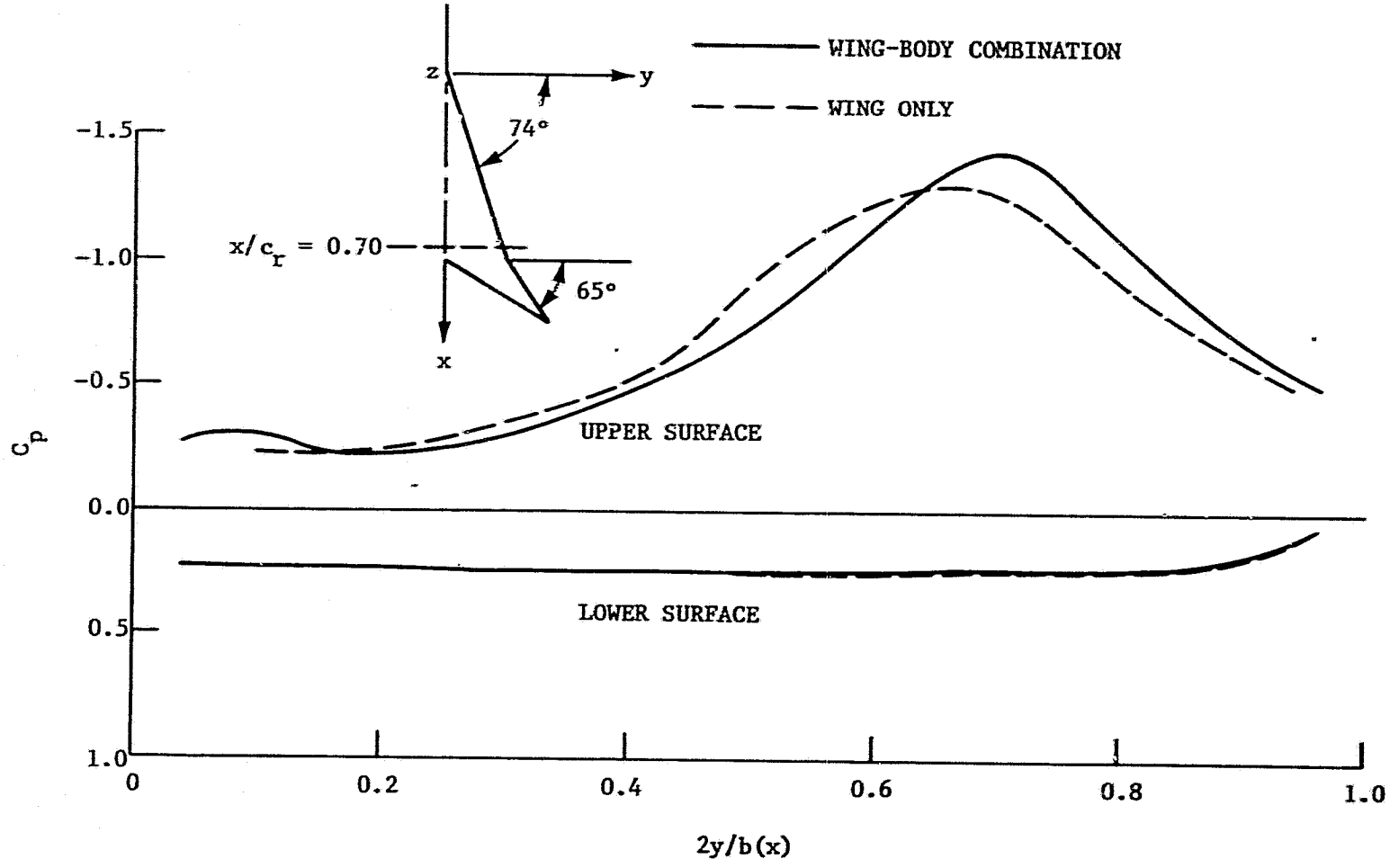

Figure 19. Comparison of spanwise pressure distributions for A = 1.72 flat double arrow wing (SCAT-15F) with and without body at $x/c_r = 0.70$, $\alpha = 20°$ and M = 0.2.

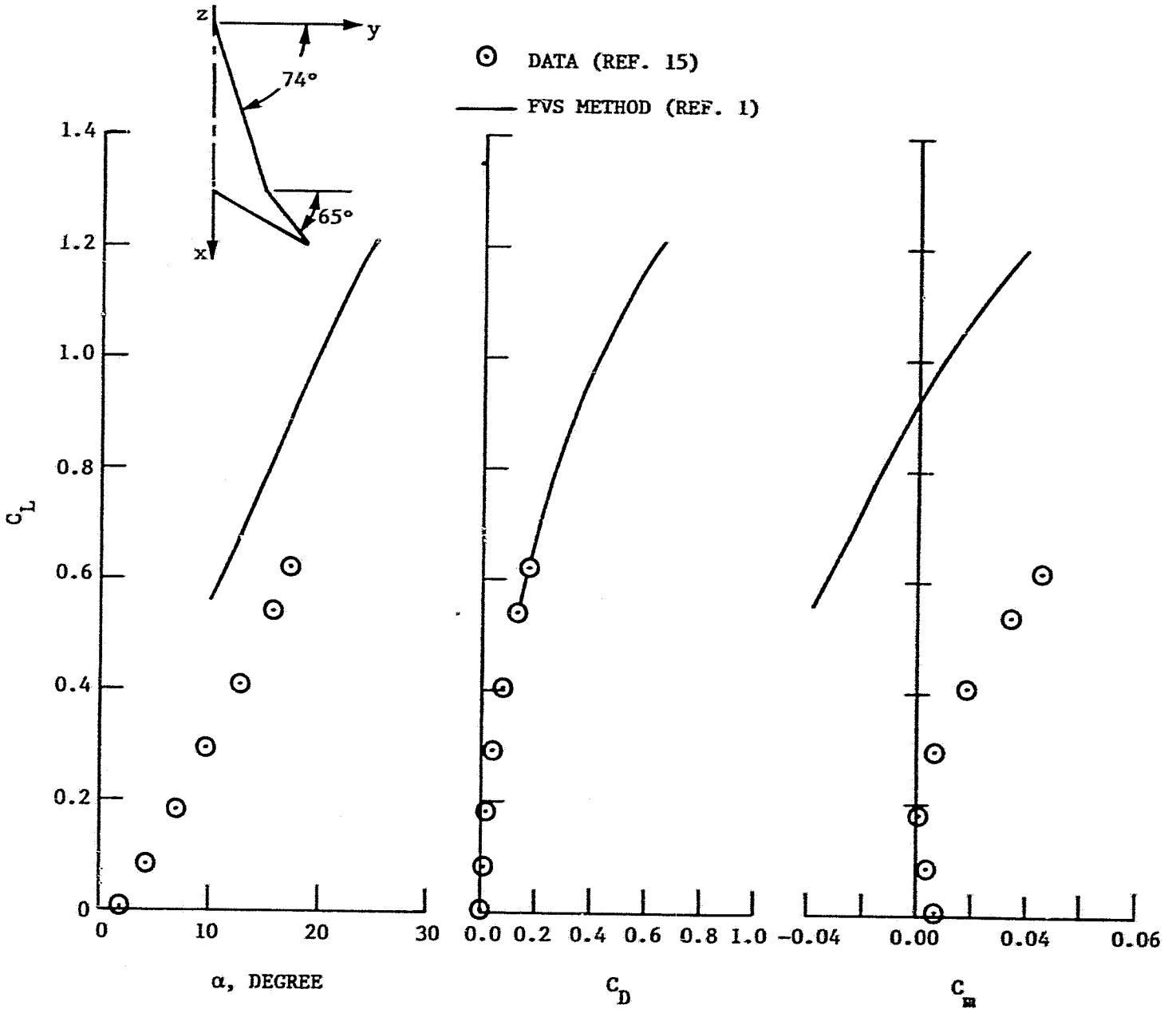

Figure 20. Aerodynamic characteristics of A = 1.72 cambered double arrow wing (SCAT-15F) at M = 0.2.

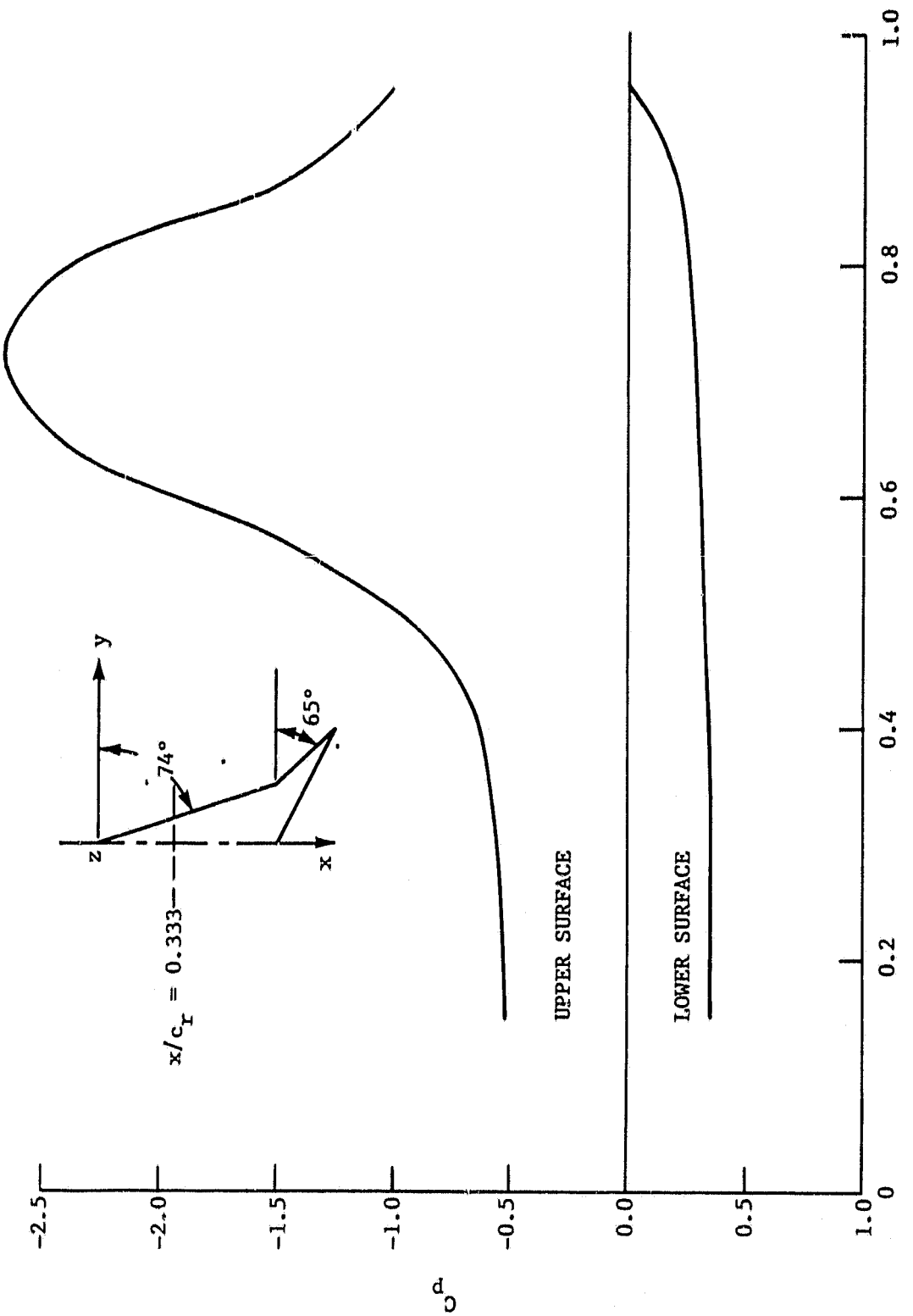

Figure 21. Spanwise pressure distributions for A = 1.72 cambered double arrow wing (SCAT-15F) at x/c_r = 0.333, α = 20° and M = 0.2.

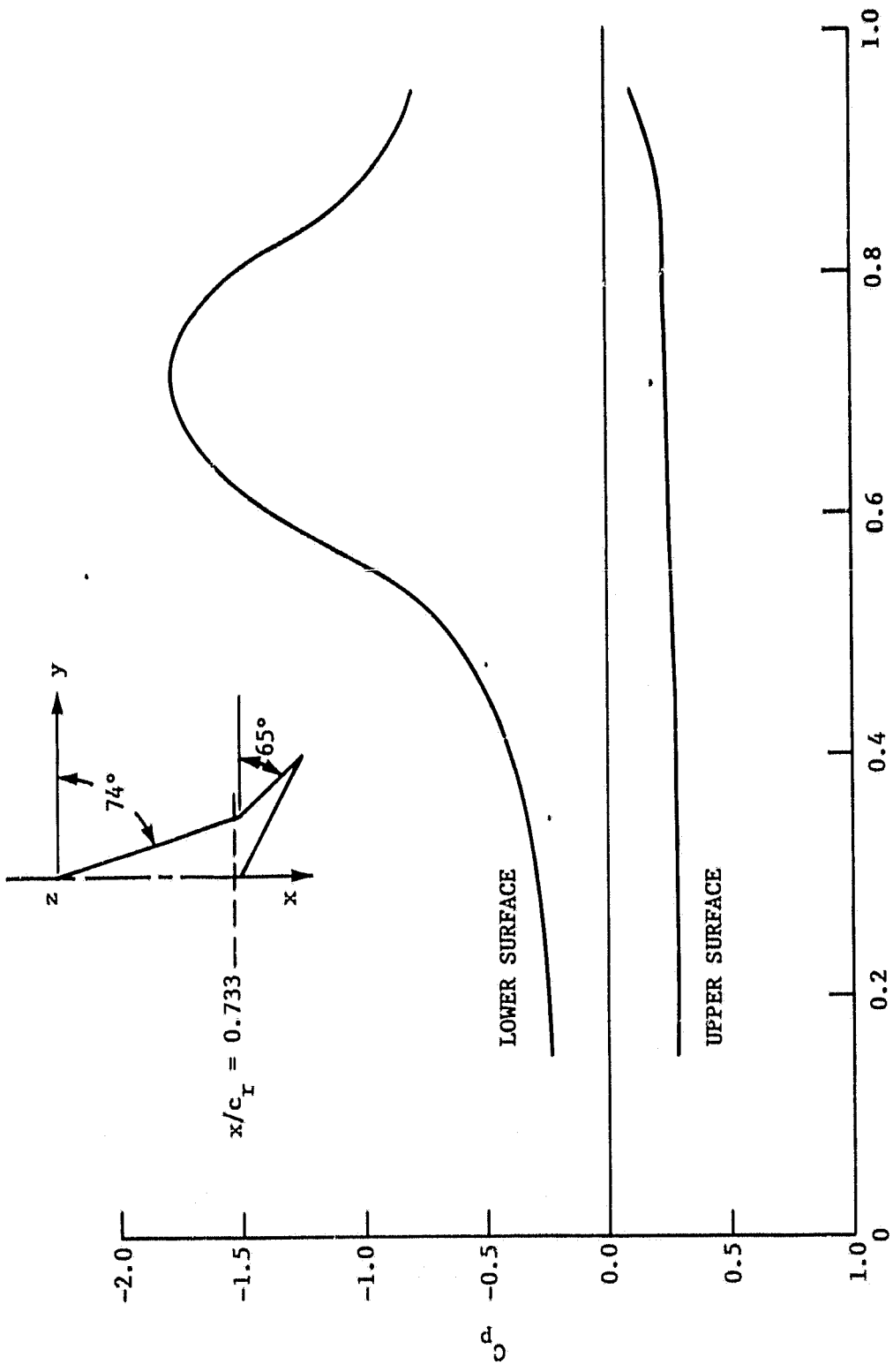

Figure 22. Spanwise pressure distributions for A = 1.72 cambered double arrow wing (SCAT-15F) at x/c_r = 0.733, α = 20° and M = 0.2.

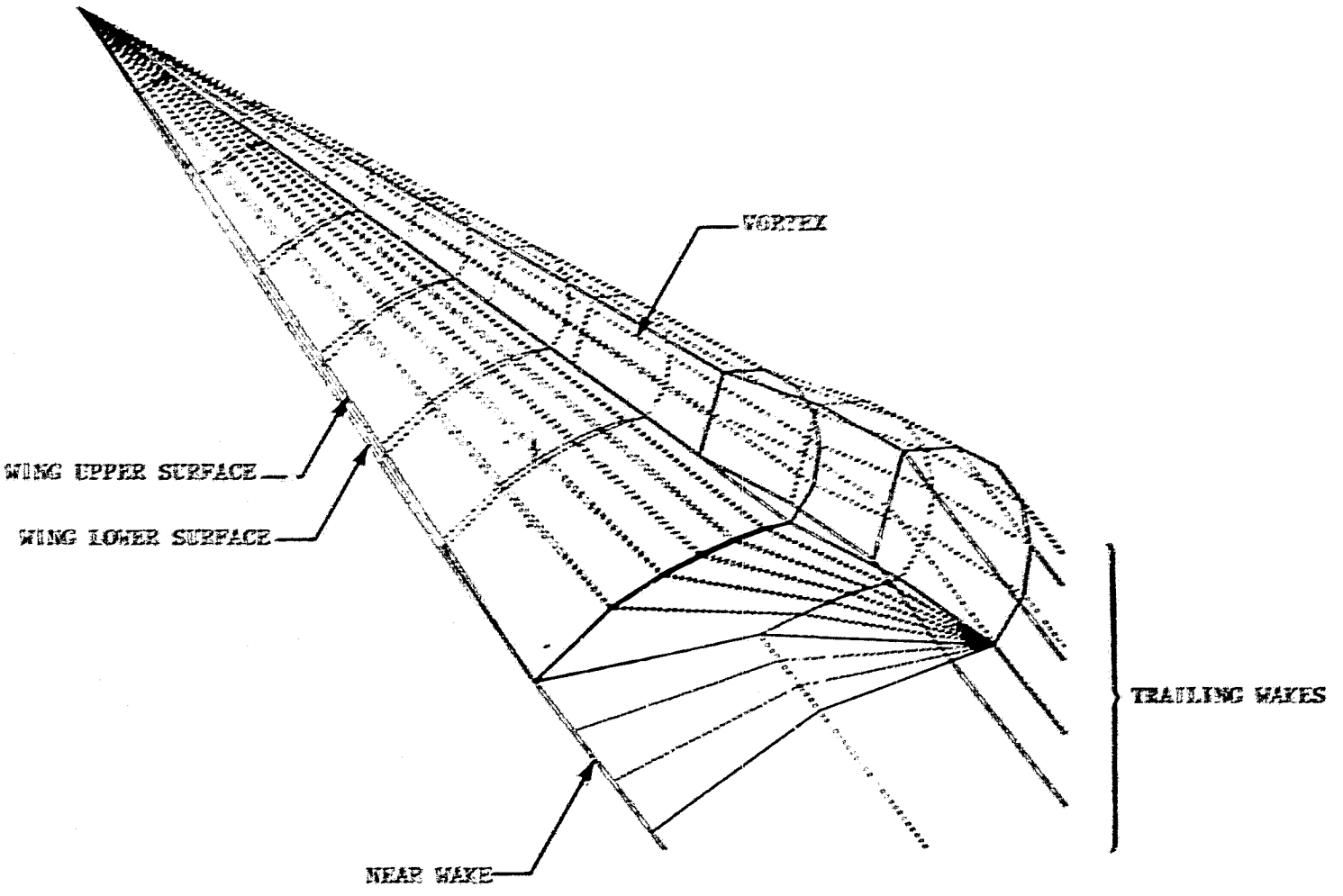

Figure 23. Cambered double arrow wing (SCAT-15F) with thickness.

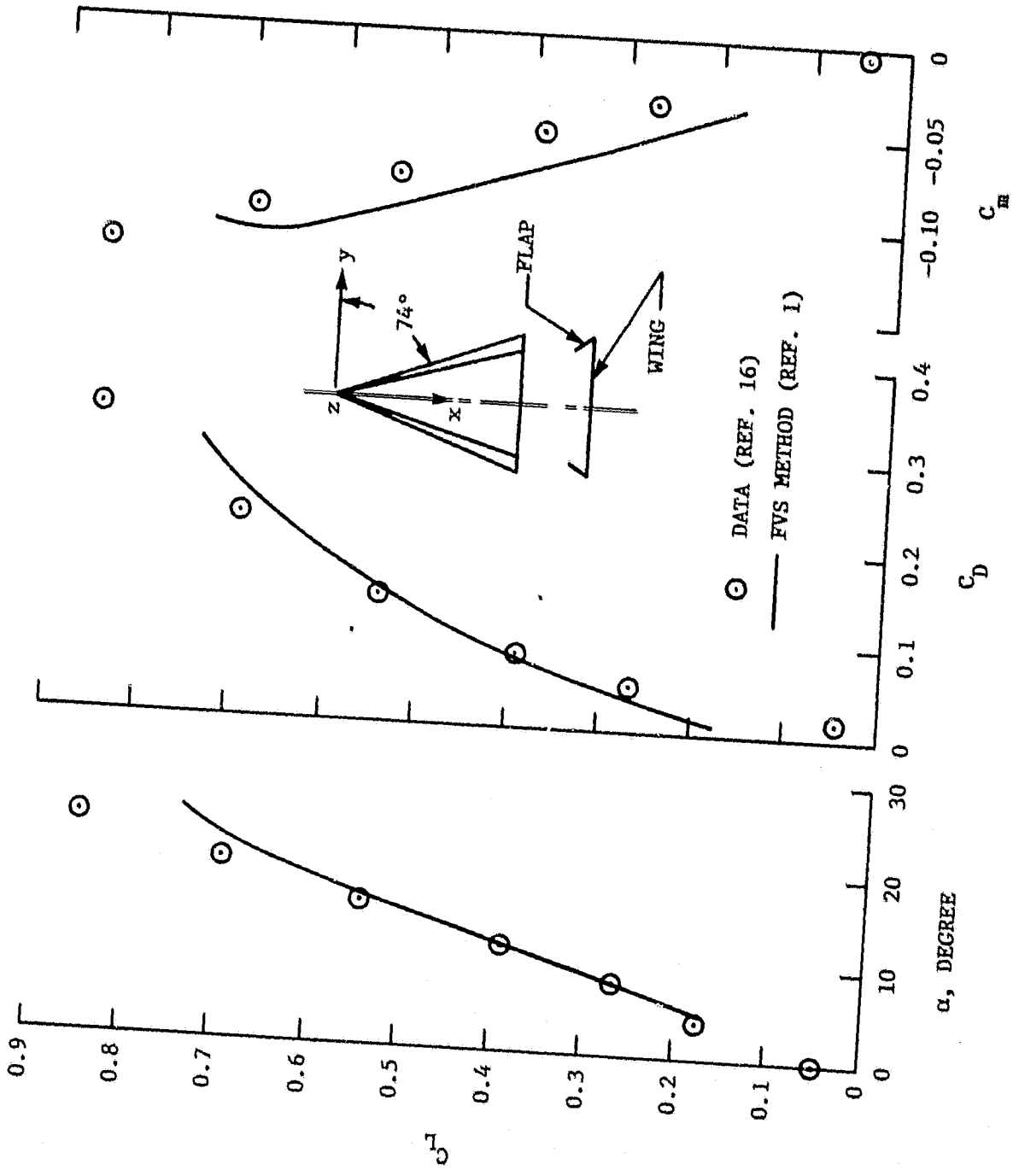

Figure 24. Longitudinal aerodynamic characteristics of A = 1.15, delta wing with δ_n = -130° leading-edge flap up at M = 0.

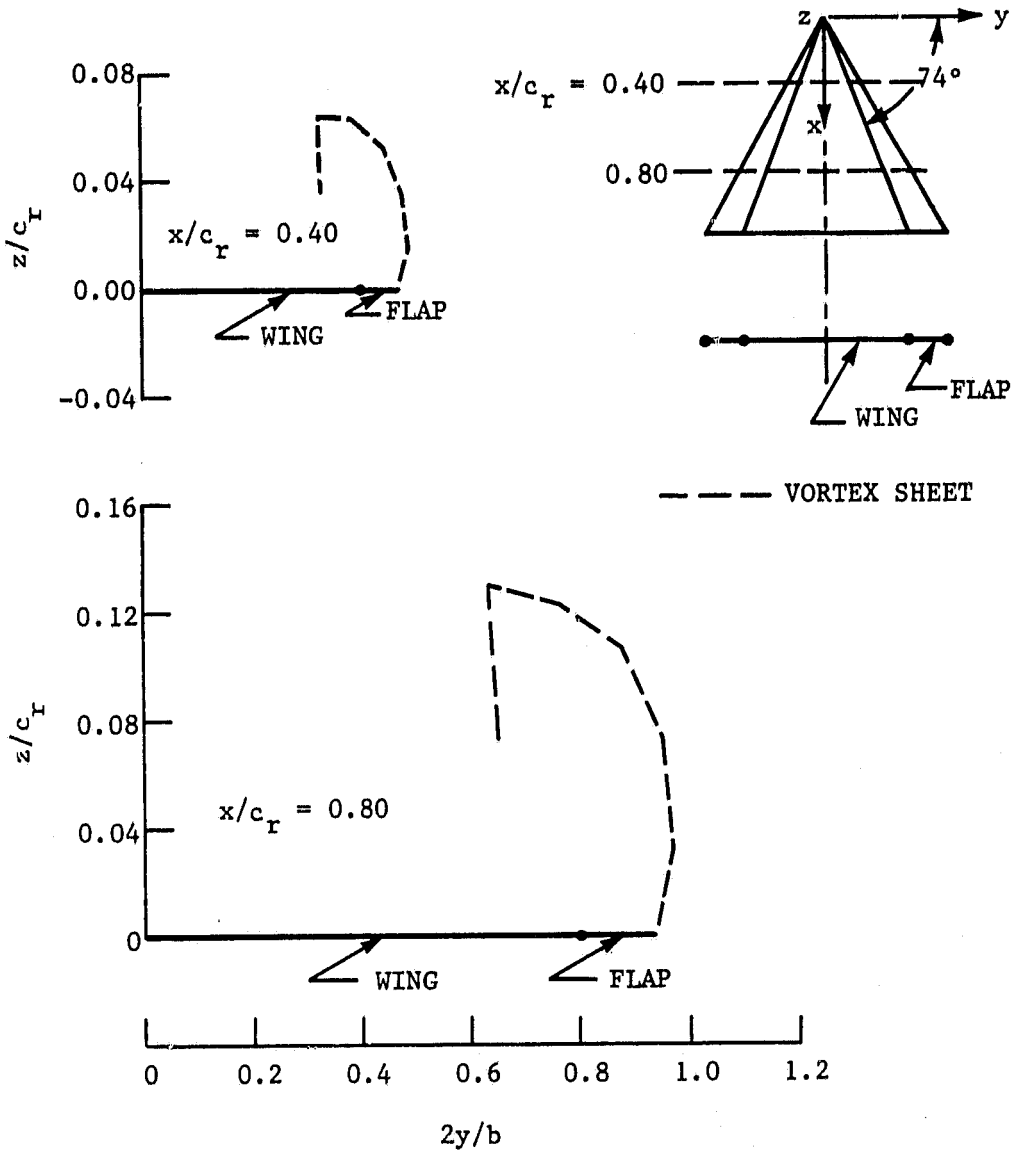

Figure 25. Converged vortex sheet shapes for A = 1.15 delta wing with no flap deflection at α = 20° and M = 0.

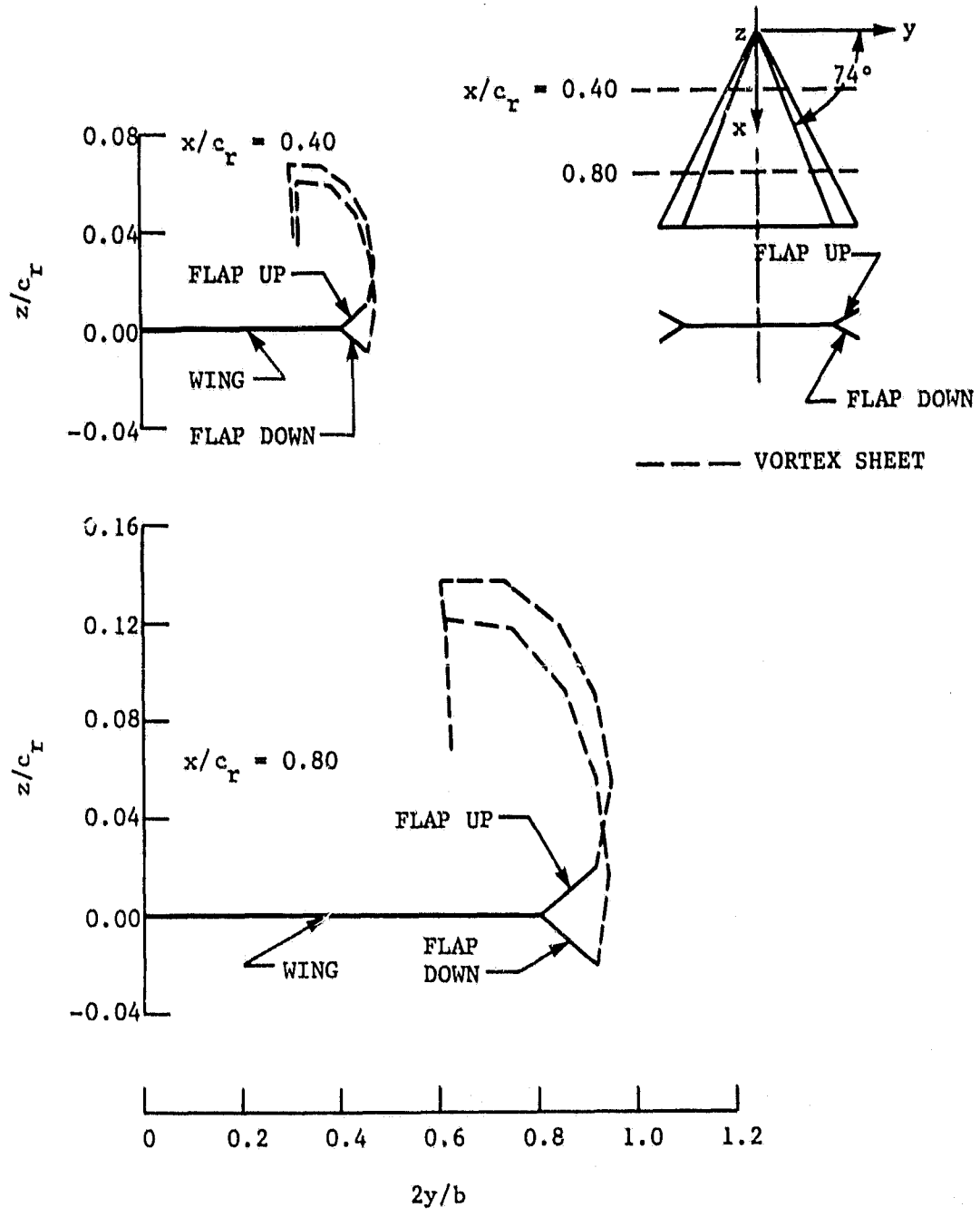

Figure 26. Converged vortex sheet shapes for A = 1.15 delta wing with $\delta_n = \pm 30°$ leading-edge flap at $\alpha = 20°$ and M = 0.

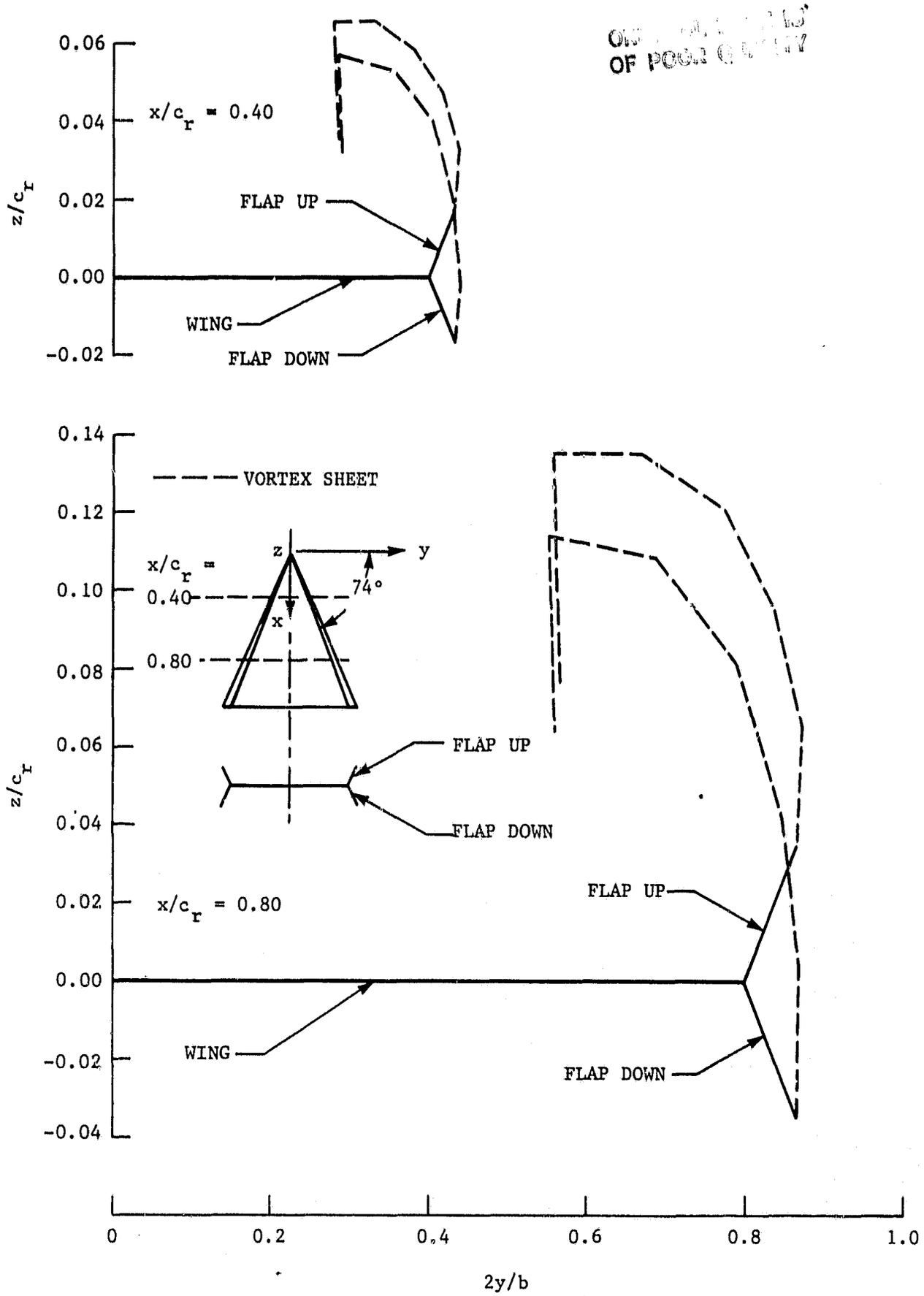

Figure 27. Converged vortex sheet shapes for A = 1.15 delta wing with $\delta_n = \pm 60°$ leading-edge flap at $\alpha = 20°$ and M = 0.

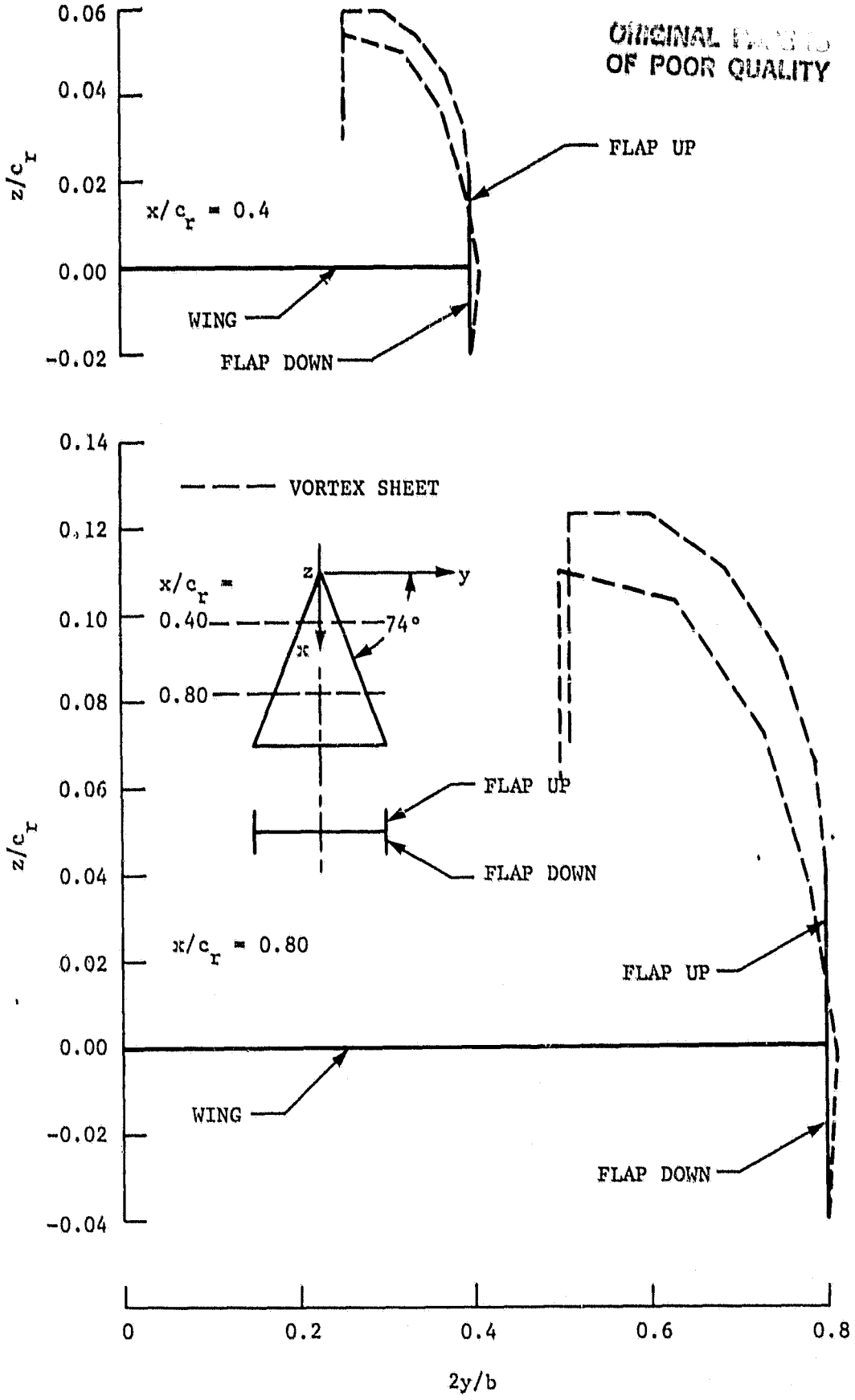

Figure 28. Converged vortex sheet shapes for A = 1.15 delta wing with $\delta_n = \pm 90°$ leading-edge flap at $\alpha = 20°$ and M = 0.

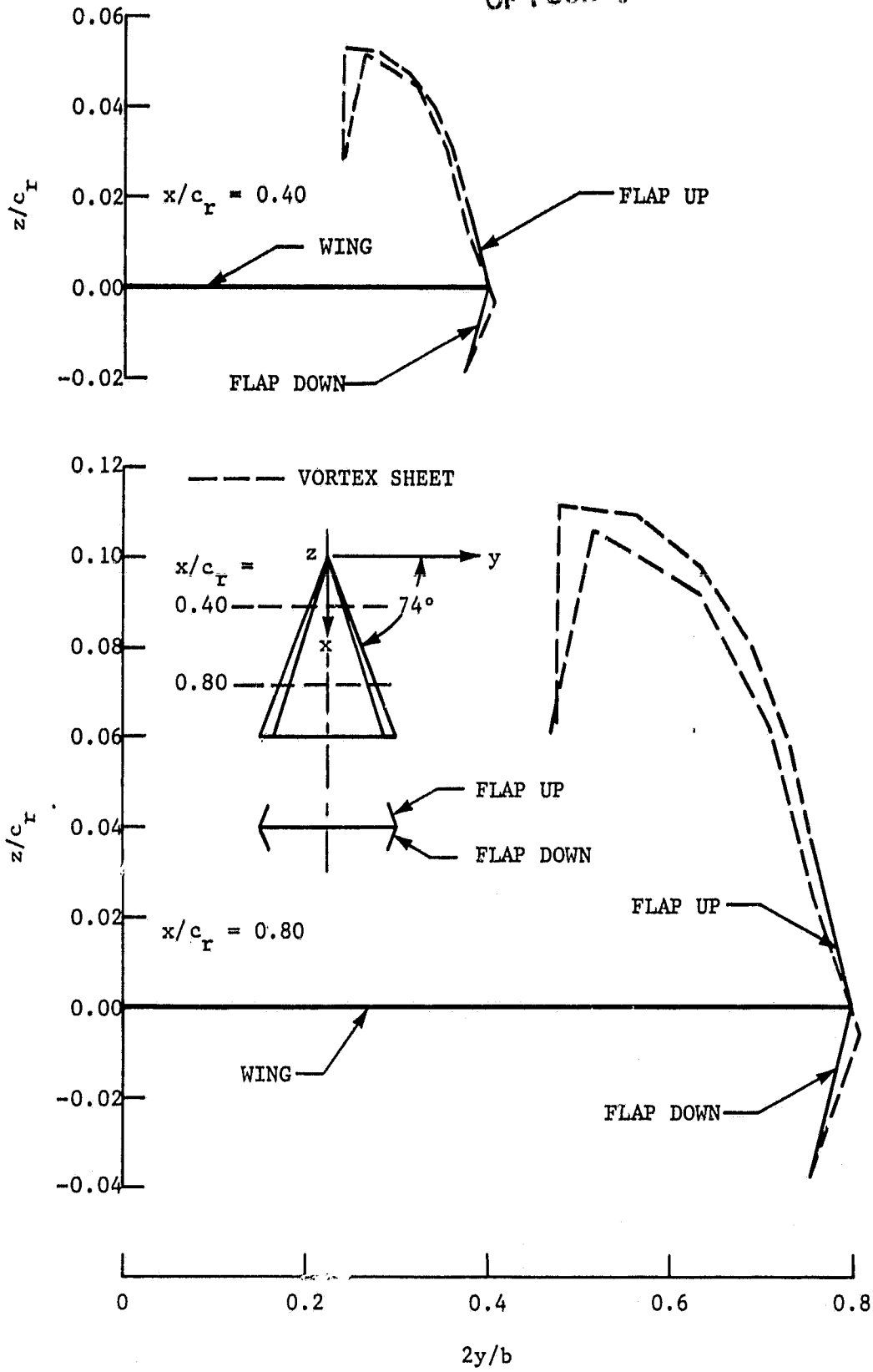

Figure 29. Converged vortex sheet shapes for A = 1.15 delta wing with $\delta_n = \pm 110°$ leading-edge flap at $\alpha = 20°$ and M = 0.

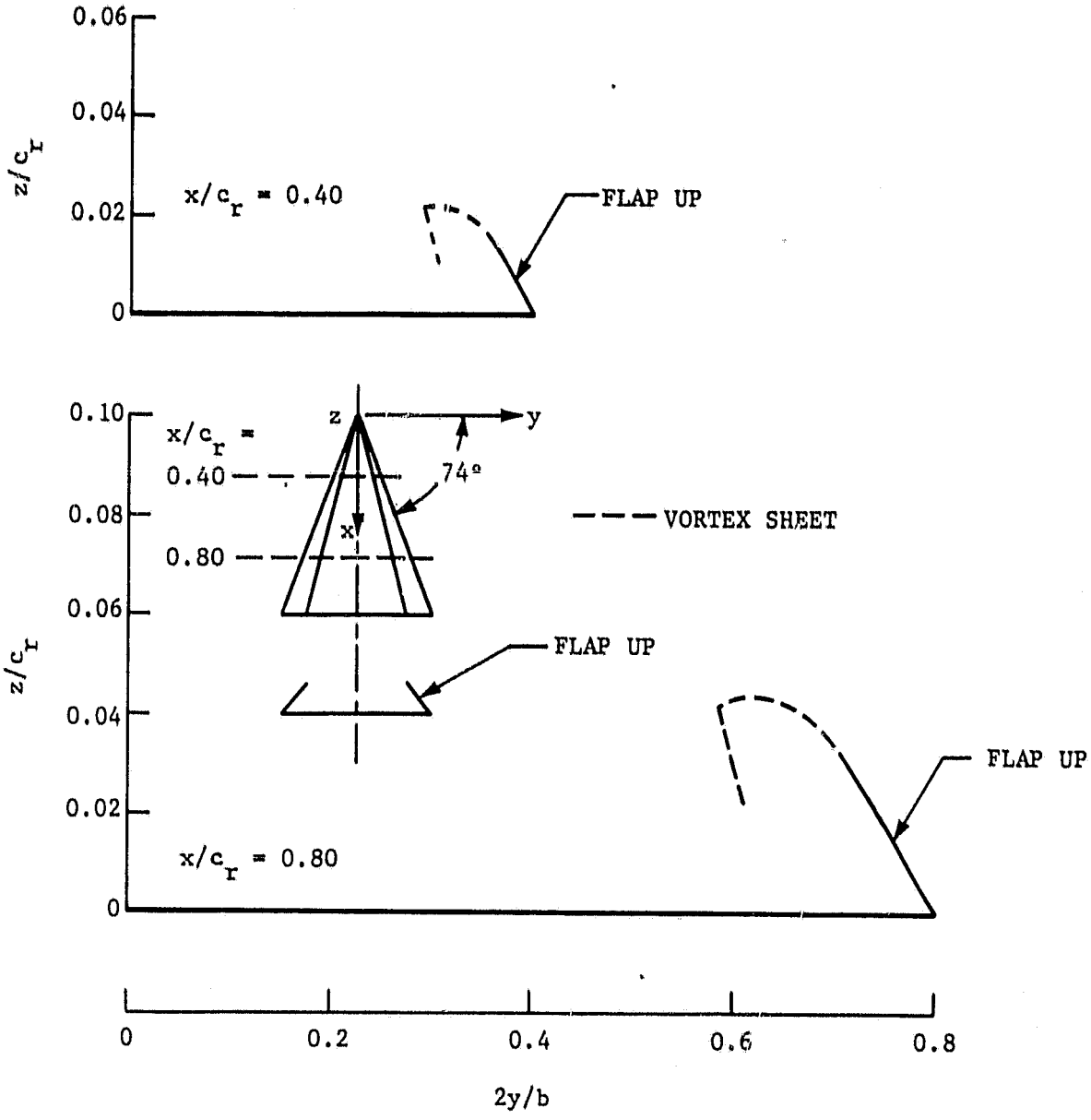

Figure 30. Converged vortex sheet shapes for A = 1.15 delta wing with δ_n = 130° leading-edge flap at α = 5° and M = 0.

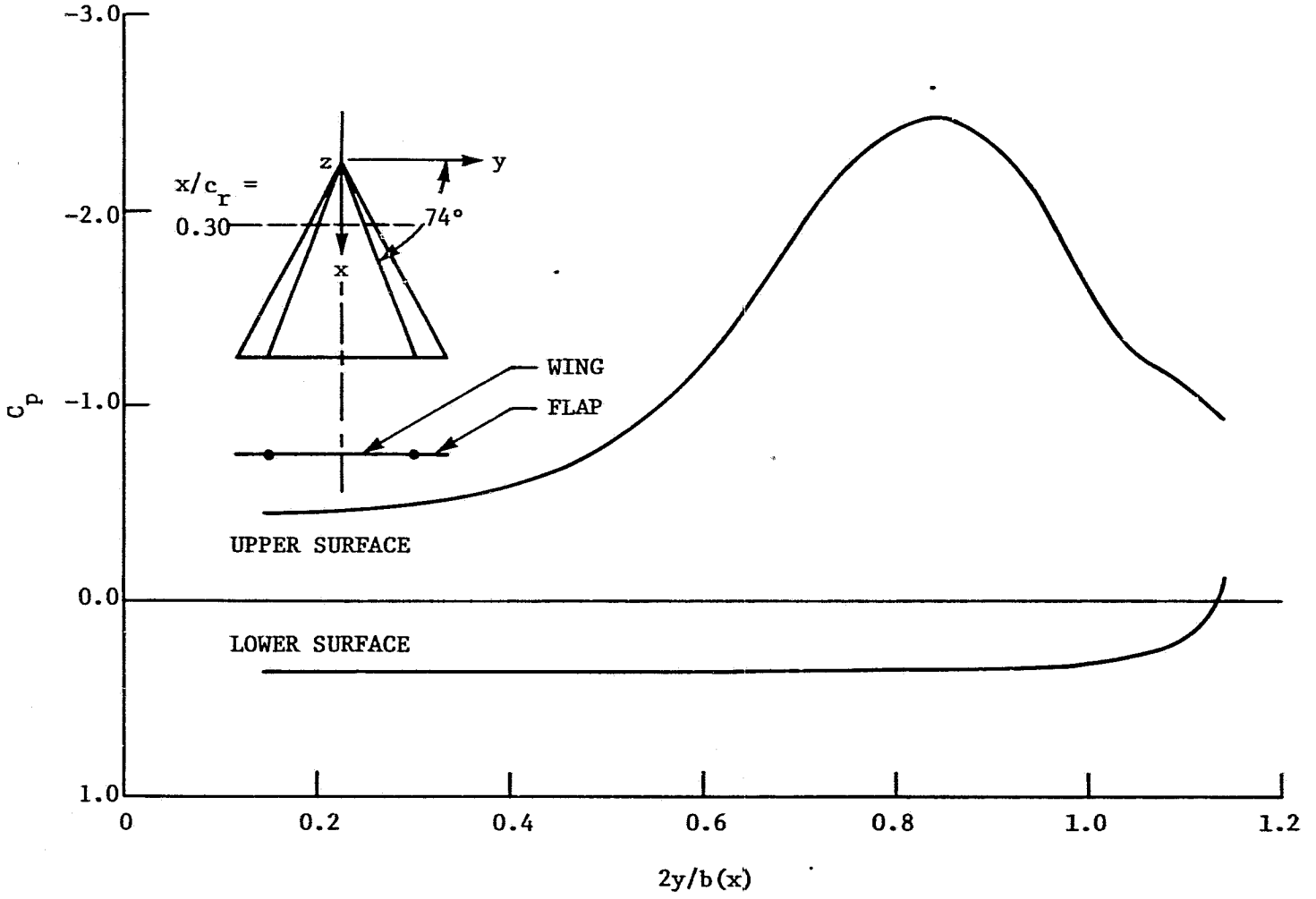

Figure 31. Spanwise pressure distributions for A = 1.15 delta wing with undeflected leading-edge flap at x/c_r = 0.30, α = 20° and M = 0.

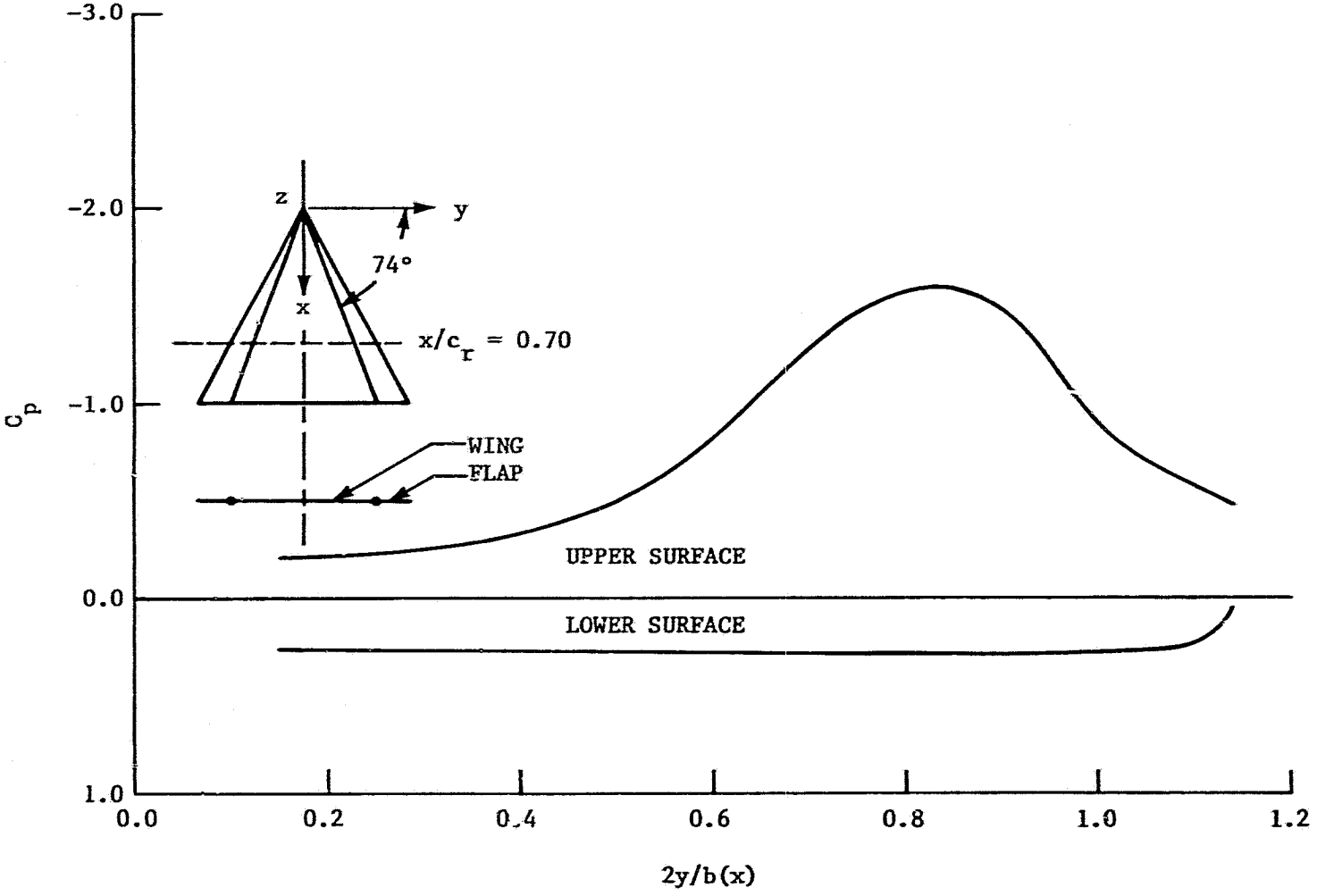

Figure 32. Spanwise pressure distributions for A = 1.15 delta wing with undeflected leading-edge flap at $x/c_r = 0.7$, $\alpha = 20°$ and M = 0.

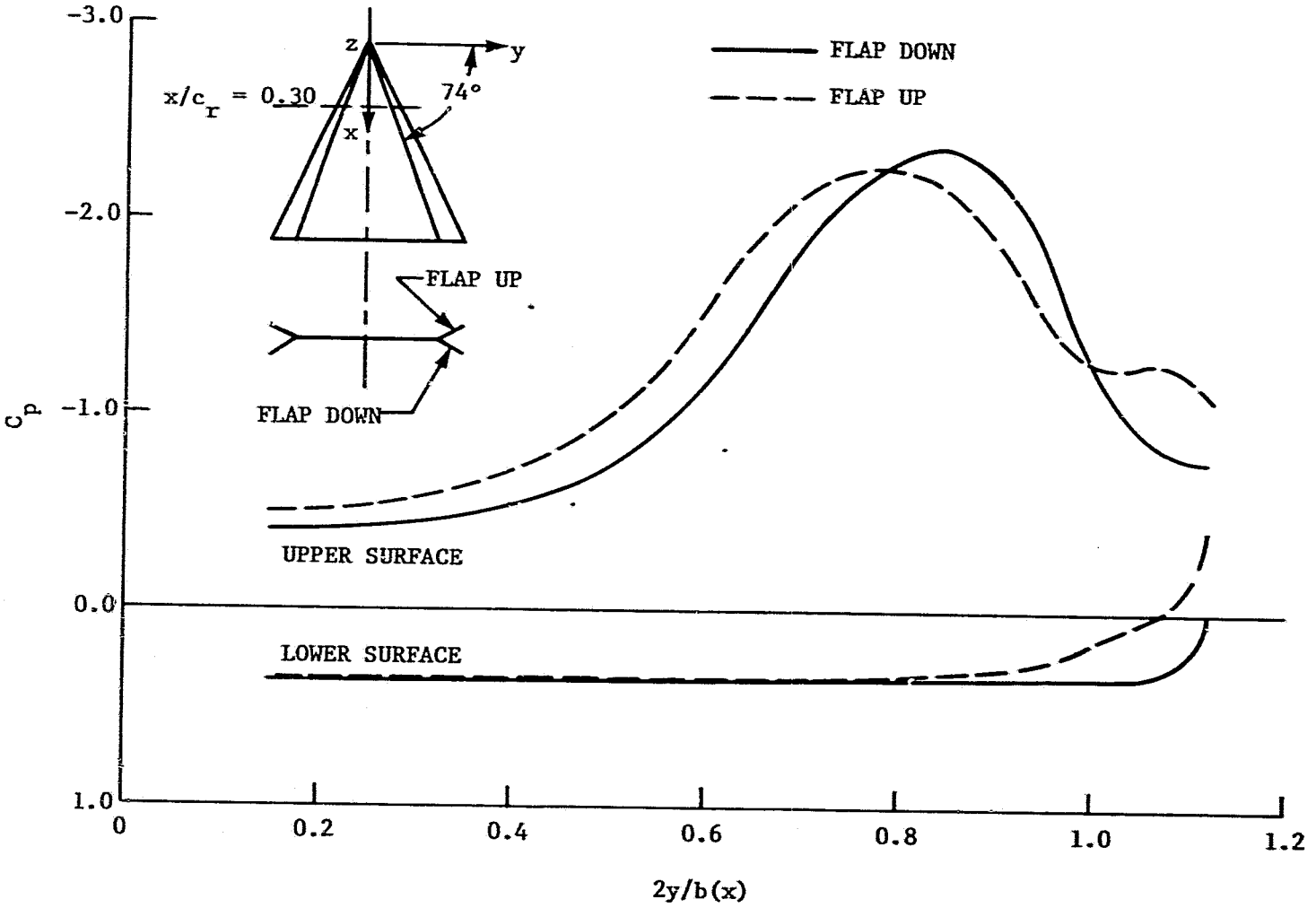

Figure 33. Spanwise pressure distributions for A = 1.15 delta wing with $\delta_n = \pm 30°$ leading-edge flap at $x/c_r = 0.30$, $\alpha = 20°$ and M = 0.

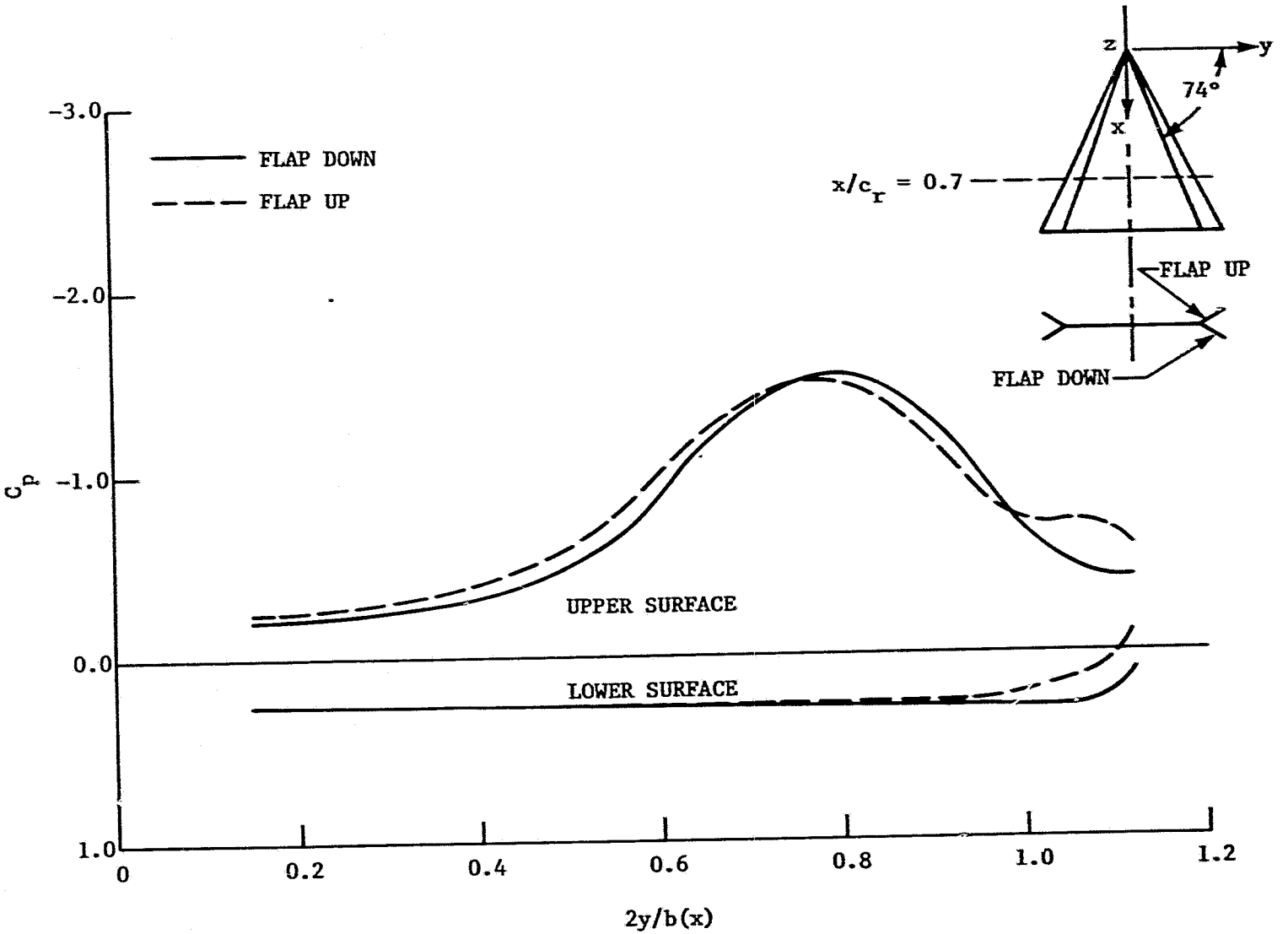

Figure 34. Spanwise pressure distributions for A = 1.15 delta wing with $\delta_n = \pm 30°$ leading-edge flap at $x/c_r = 0.70$, $\alpha = 20°$ and M = 0.

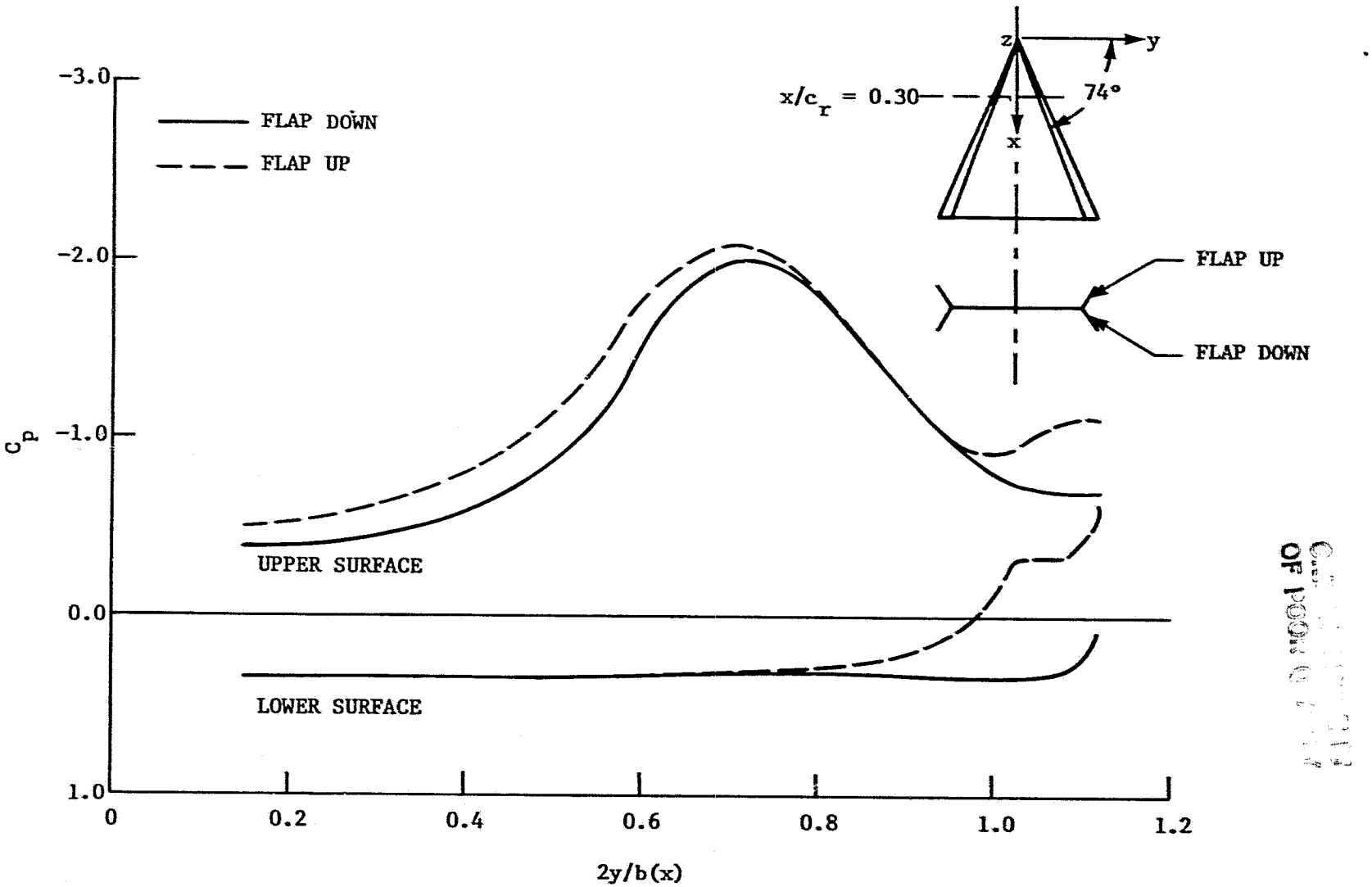

Figure 35. Spanwise pressure distributions for A = 1.15 delta wing with $\delta_n = \pm 60°$ leading-edge flap at $x/c_r = 0.30$, $\alpha = 20°$ and M = 0.

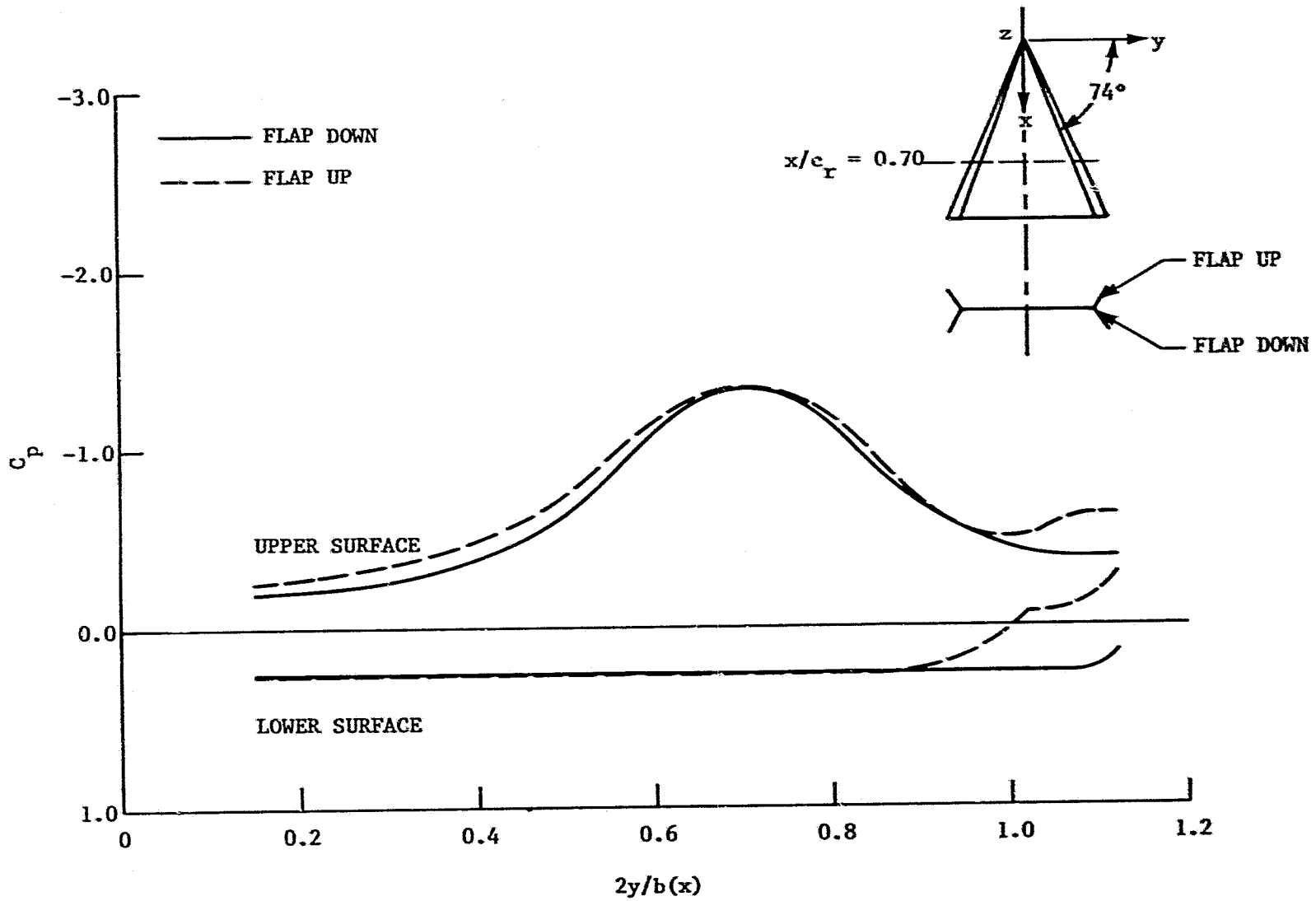

Figure 36. Spanwise pressure distributions for A = 1.15 delta wing with $\delta_n = \pm 60°$ leading-edge flap at $x/c_r = 0.70$, $\alpha = 20°$ and M = 0.

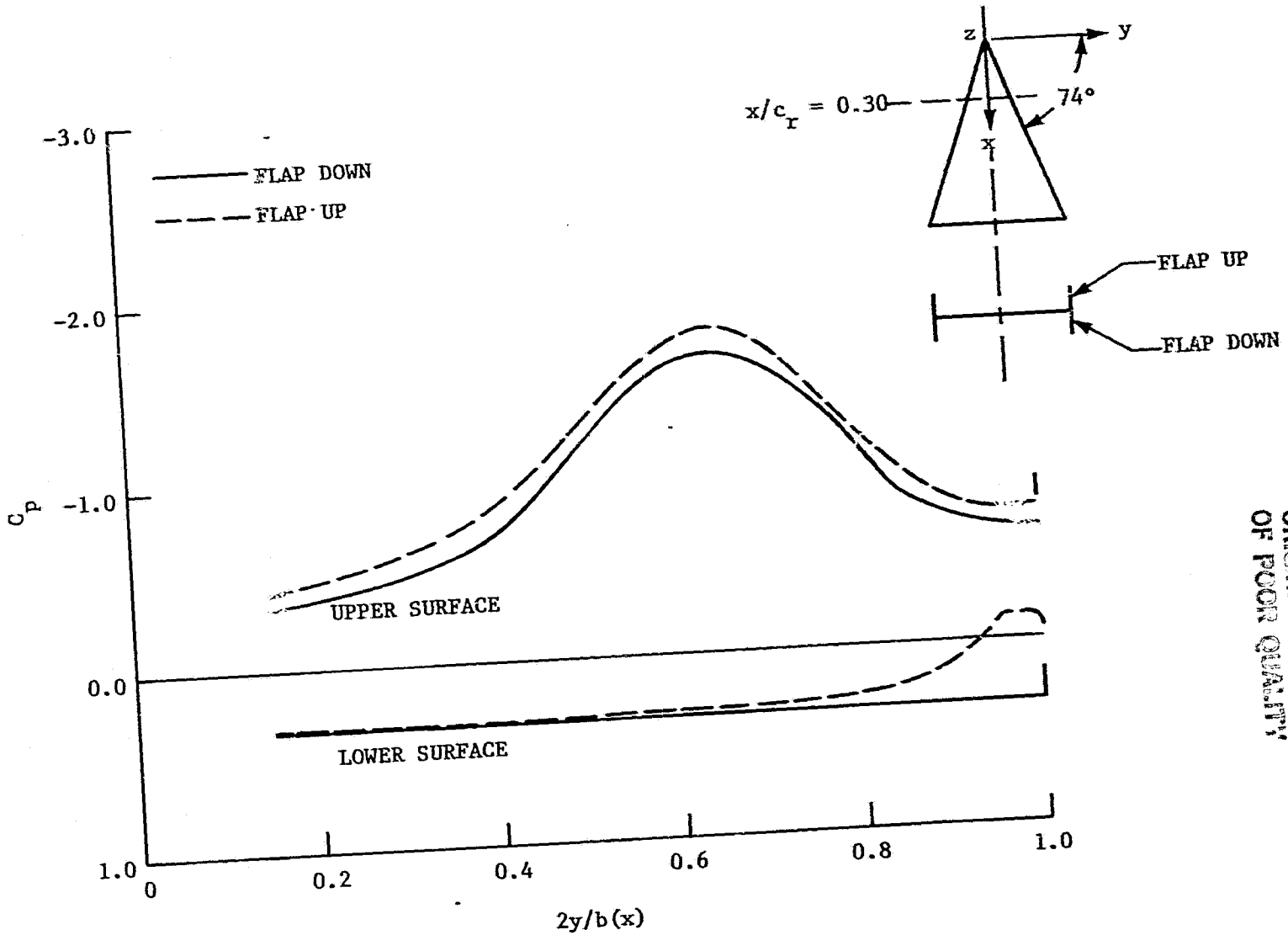

Figure 37. Spanwise pressure distributions for A = 1.15 delta wing with $\delta_n = \pm 90°$ leading-edge flap at $x/c_r = 0.30$, $\alpha = 20°$ and M = 0.

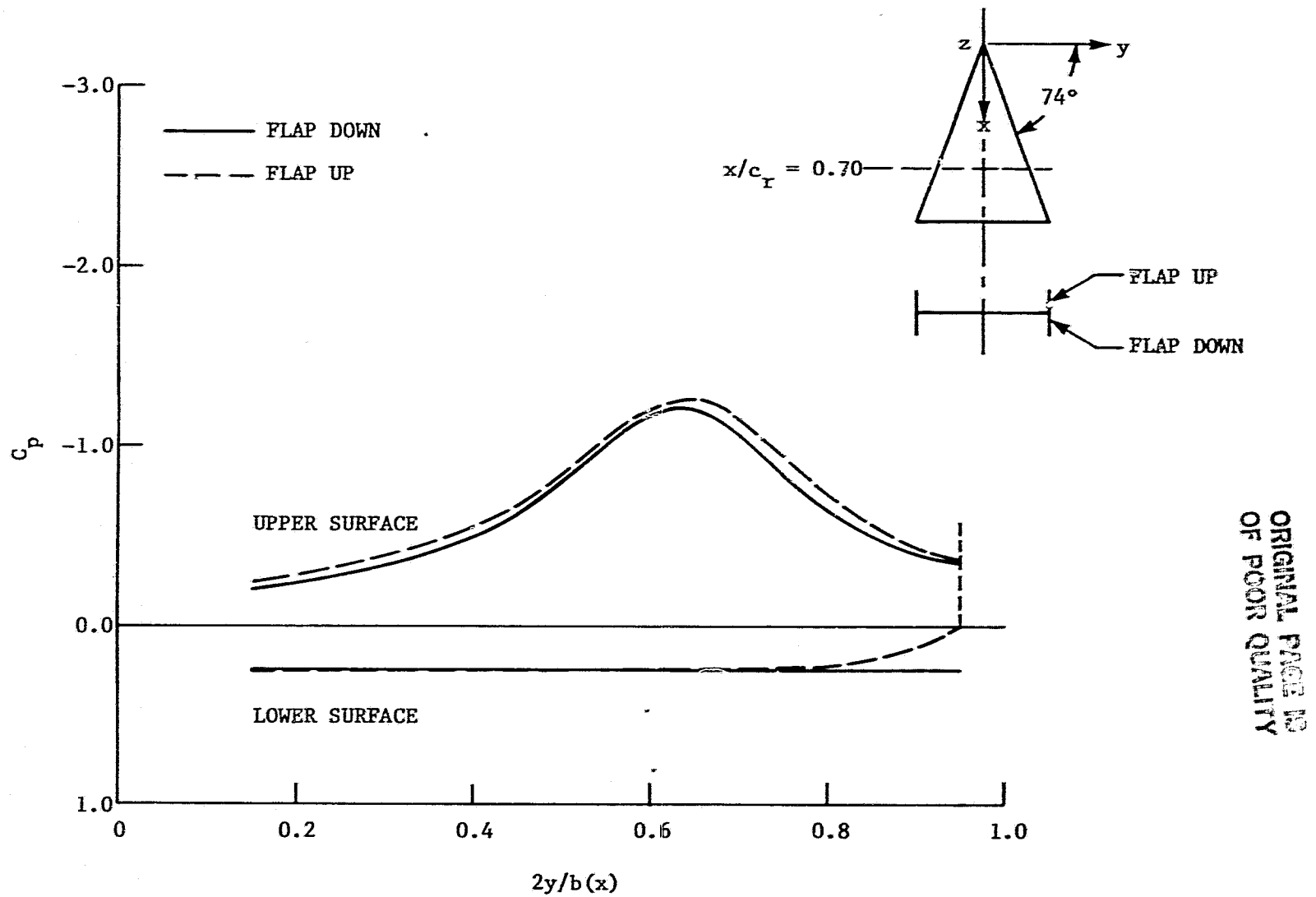

Figure 38. Spanwise pressure distributions for A = 1.15 delta wing with $\delta_n = \pm 90°$ leading-edge flap at $x/c_r = 0.70$, $\alpha = 20°$ and M = 0.

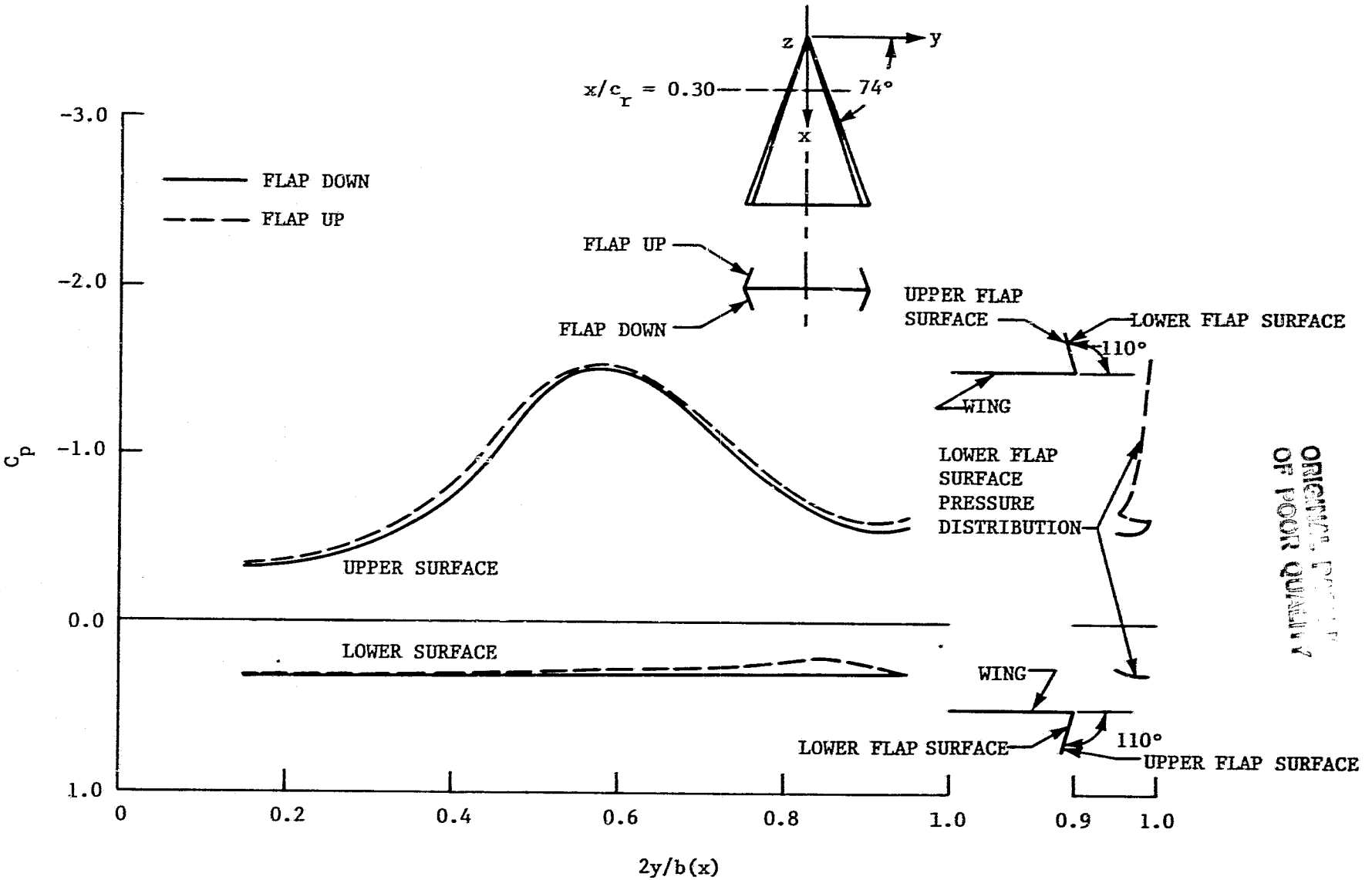

Figure 39. Spanwise pressure distributions for A = 1.15 delta wing with $\delta_n = \pm 110°$ leading-edge flap at $x/c_r = 0.30$, $\alpha = 20°$ and M = 0.

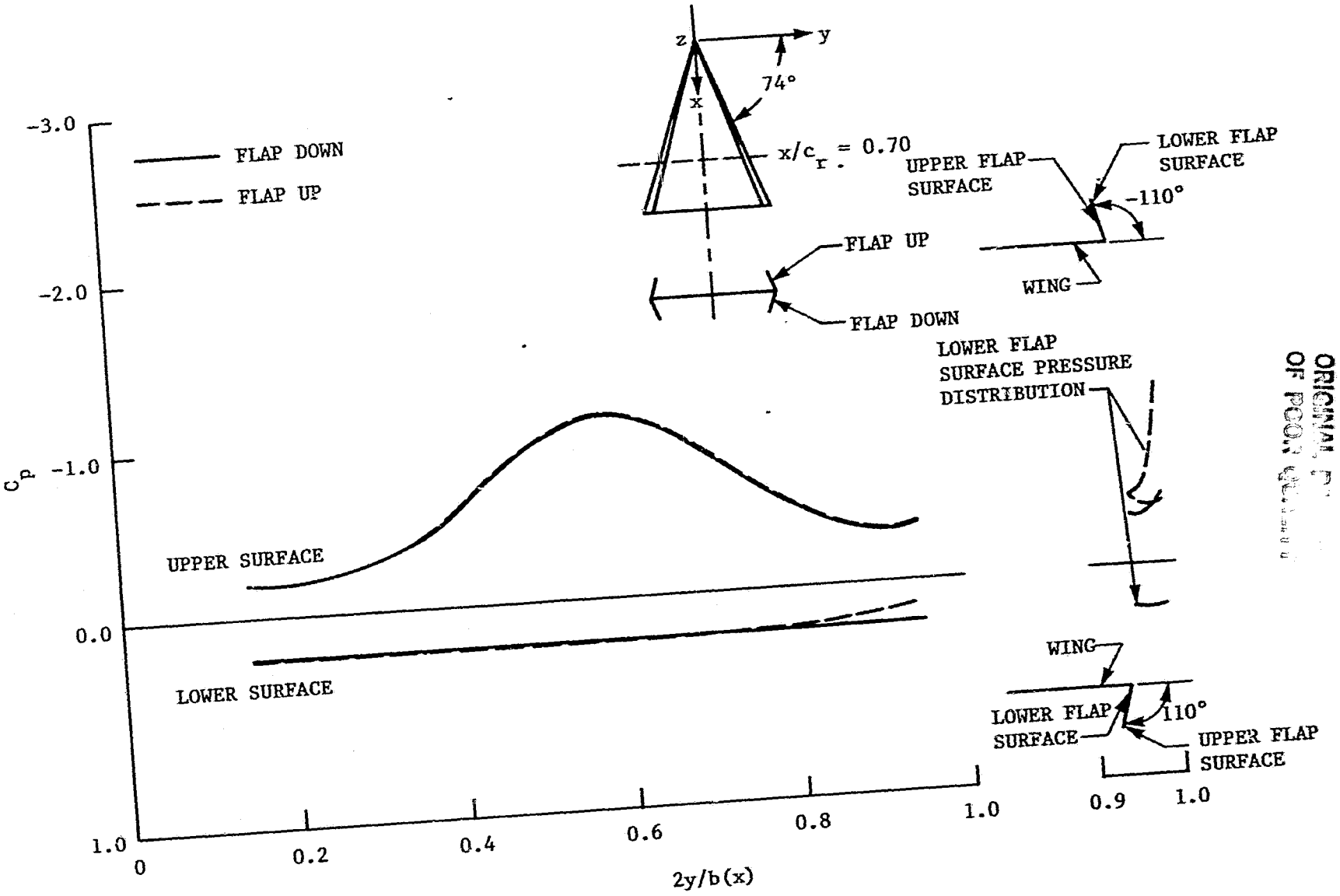

Figure 40. Spanwise pressure distributions for A = 1.15 delta wing with $\delta_n = \pm 110°$ leading-edge flap at $x/c_r = 0.70$, $\alpha = 20°$ and M = 0.

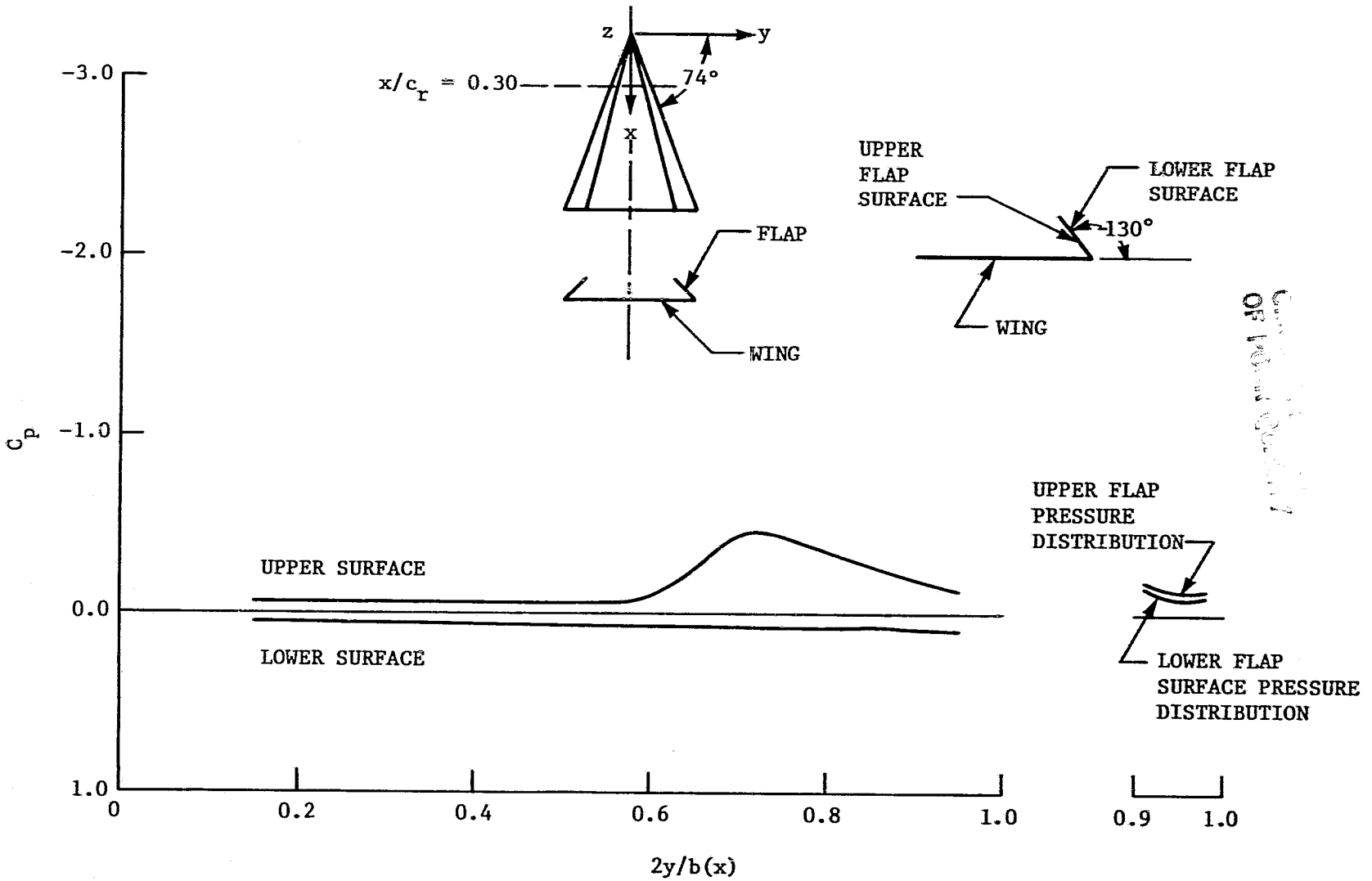

Figure 41. Spanwise pressure distributions for A = 1.15 delta wing with δ_n = -130° leading-edge flap at x/c_r = 0.30, α = 5.0° and M = 0.

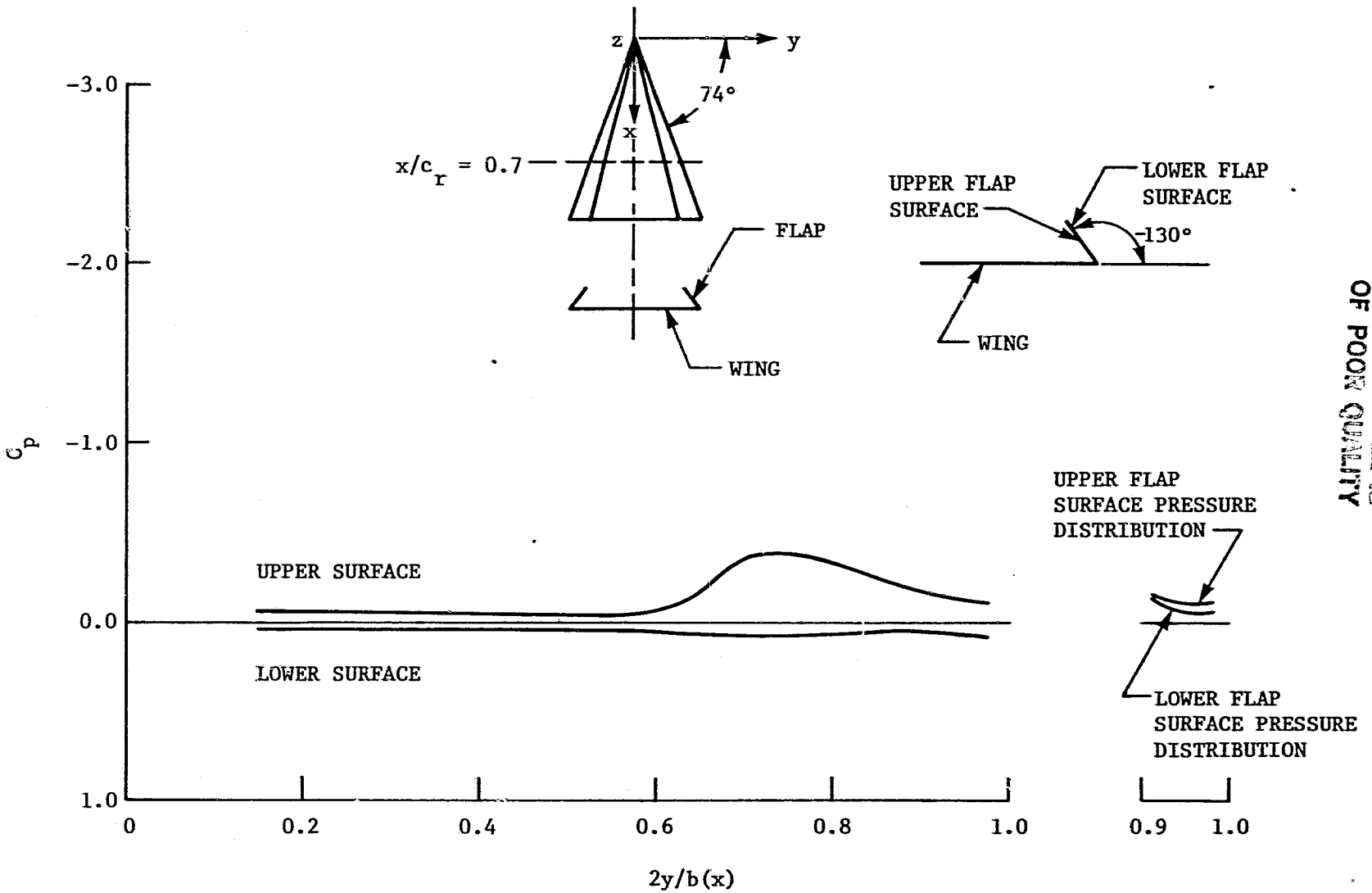

Figure 42. Spanwise pressure distributions for A = 1.15 delta wing with δ_n = -130° leading-edge flap at x/c_r = 0.70, α = 5.0° and M = 0.

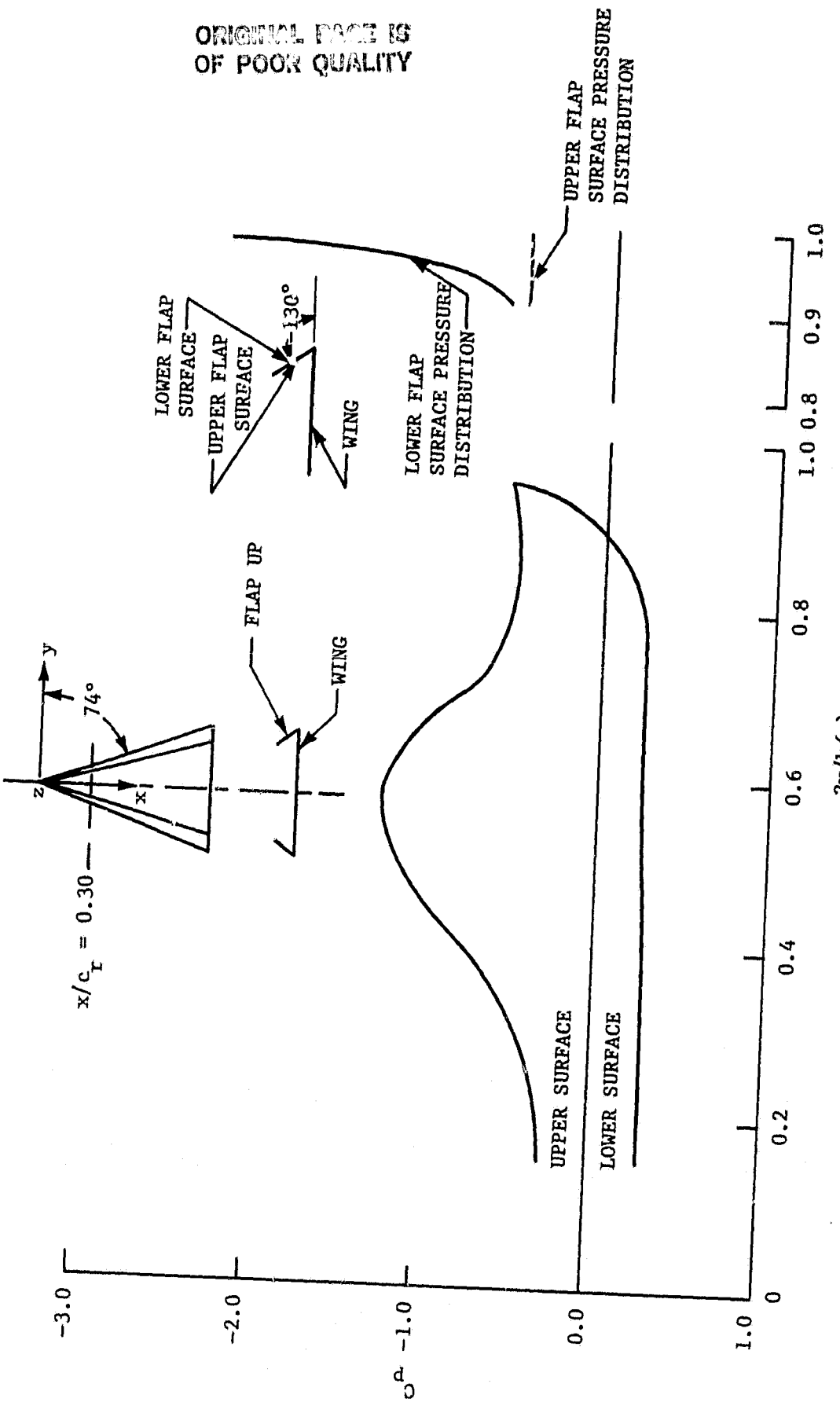

Figure 43. Spanwise pressure distributions for A = 1.15 delta wing with δ_n =-130° leading-edge flap at x/c_r = 0.30, α = 20° and M = 0.

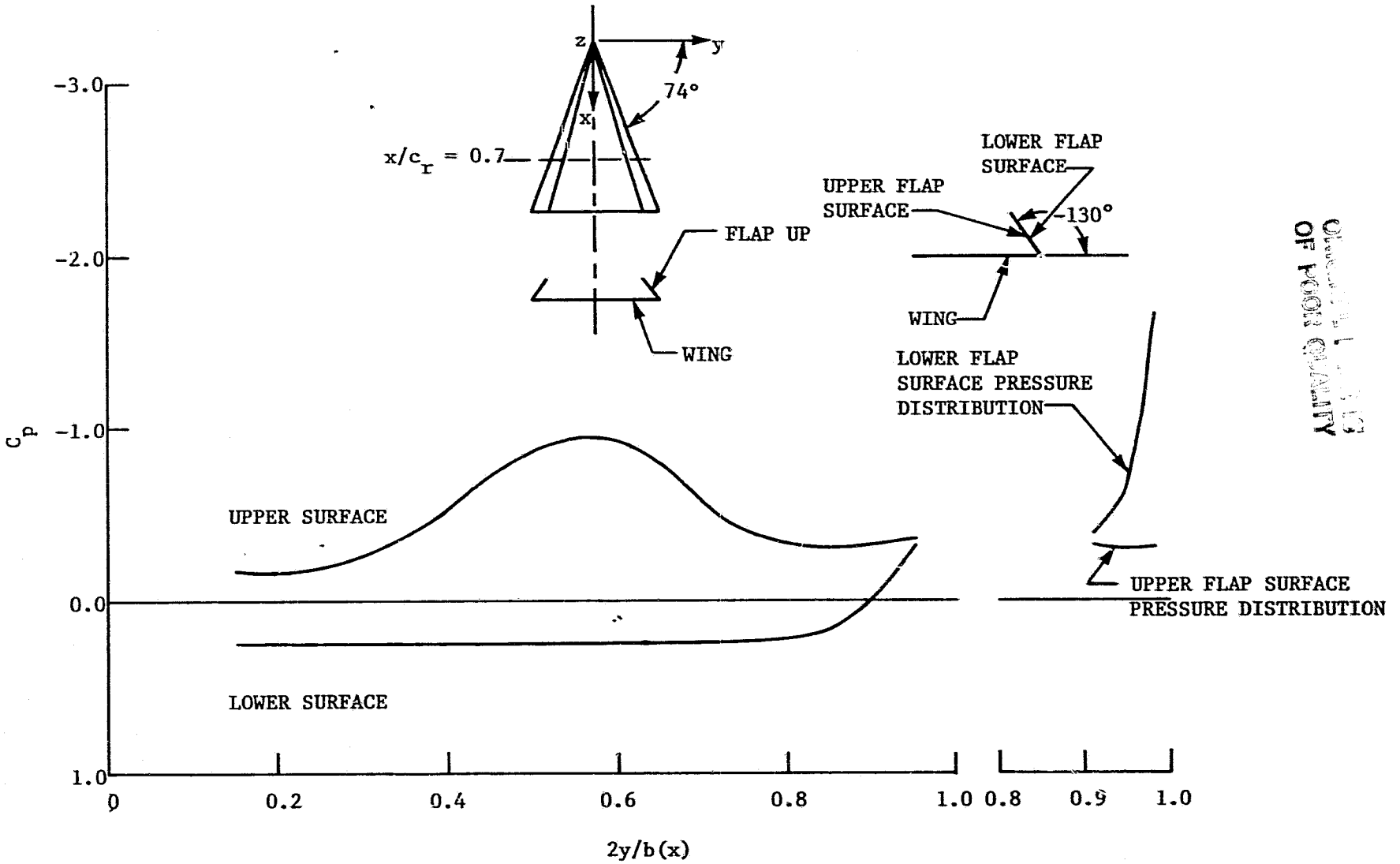

Figure 44. Spanwise pressure distributions for A = 1.15 delta wing with δ_n = -130° leading-edge flap at x/c_r = 0.70, α = 20° and M = 0.

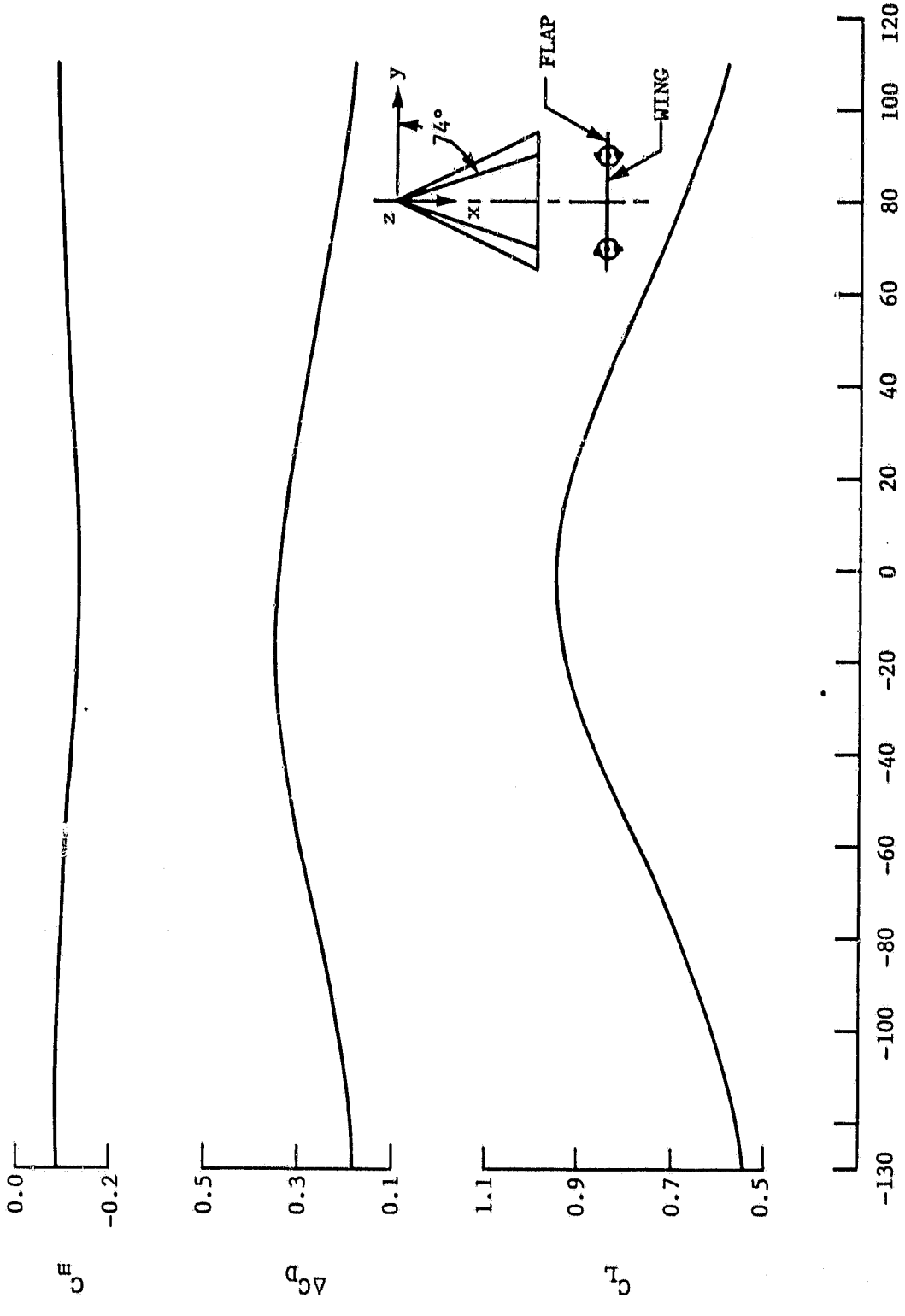

Figure 45. Effect of flap deflection on longitudinal aerodynamic characteristics for A = 1.15 delta wing at α = 20° and M = 0.

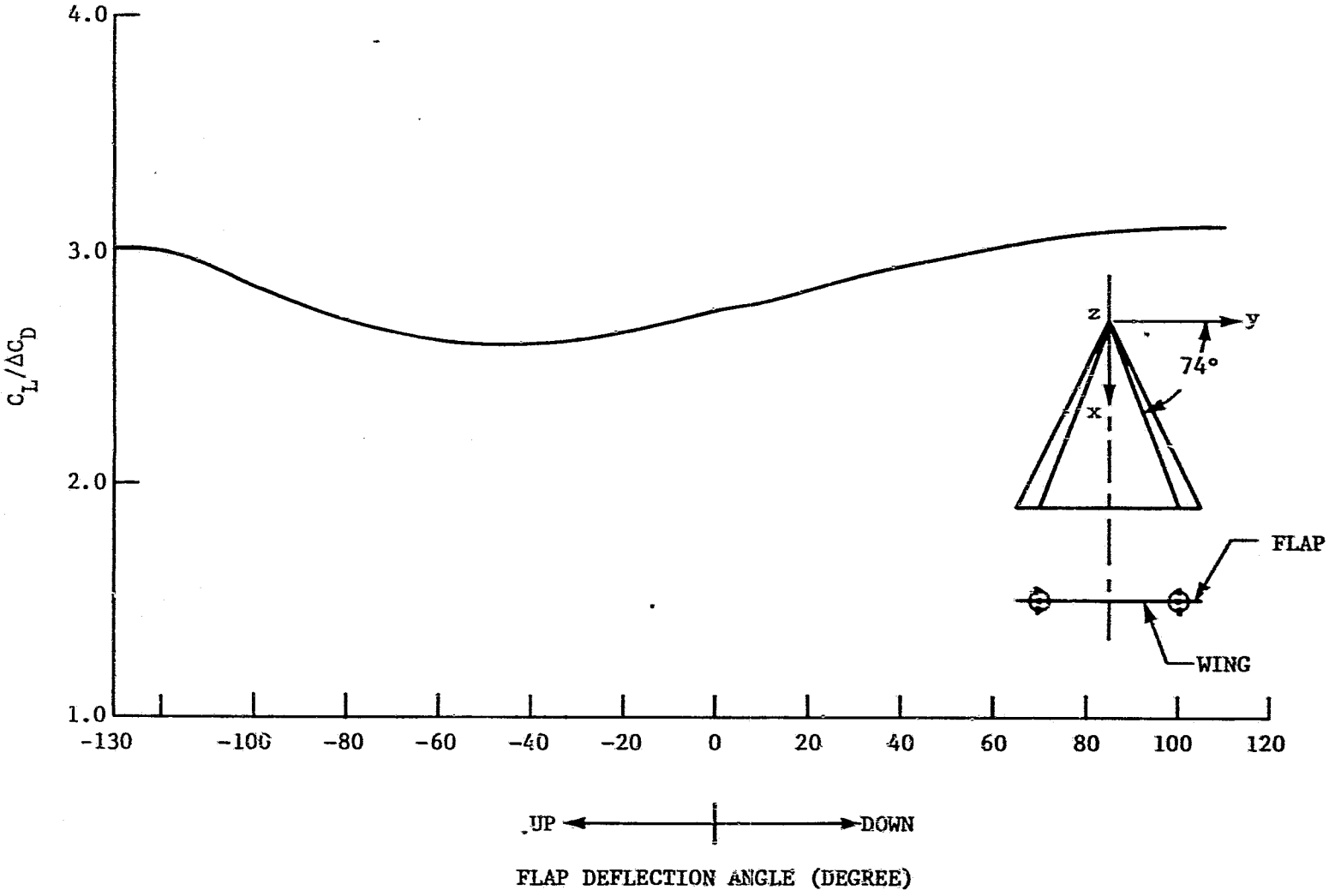

Figure 46. Effect of flap deflection on lift-to-drag ratio for A = 1.15 delta wing at α = 20° and M = 0.

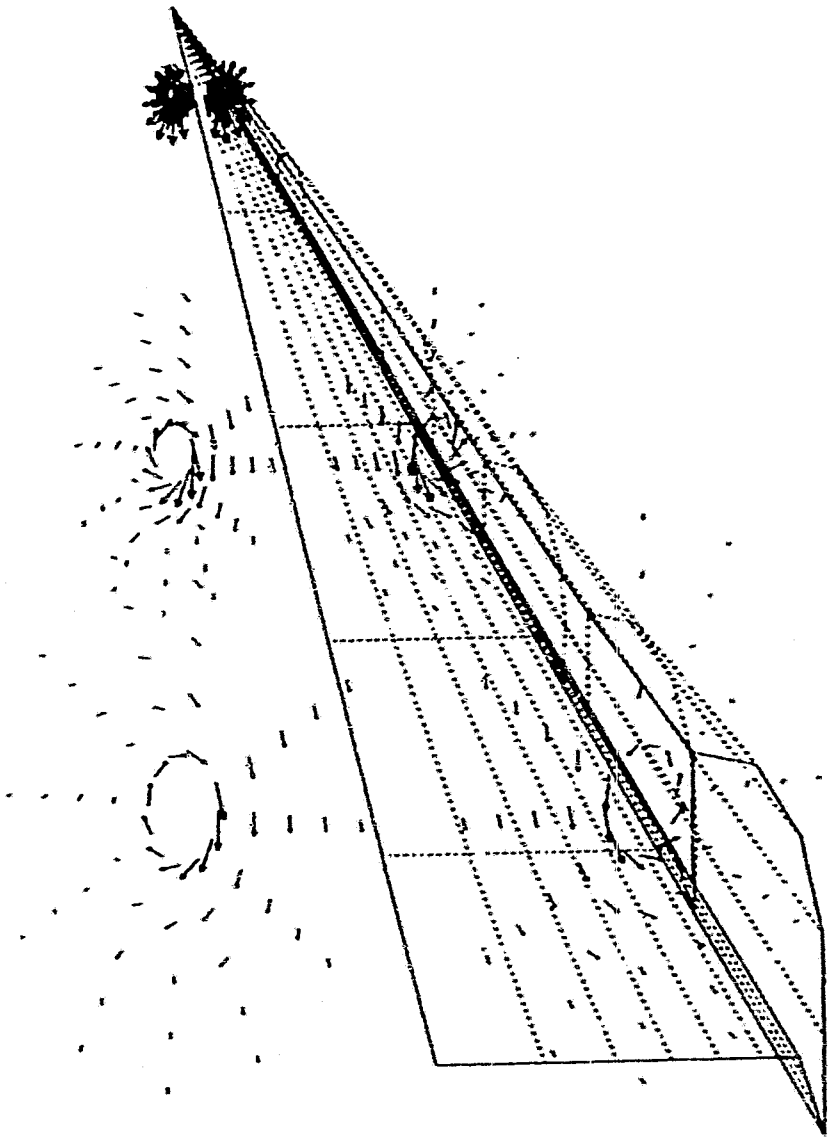

Figure 47. Vortex flow pattern on A = 1.15 delta wing with δ_n = 60° leading-edge flap at α = 20° and M = 0.